Chapter 9

Recombination Radiation in the Diamond

Evgeniy Igorevich Lipatov,
Dmitriy Evgen'evich Genin,
Denis Valer'evich Grigor'ev and
Victor Fedotovich Tarasenko

Additional information is available at the end of the chapter

http://dx.doi.org/10.5772/65064

Abstract

Original experimental data on the recombination radiation of free excitons, the band-A of luminescence, and the recombination radiation of electron-hole liquid in a diamond have been presented. A review of the literature on the recombination radiation in diamond and its application was performed. There was no displacement of free-exciton band at 5.275 eV in the temperature range of 80–300 K. At low excitation levels, the temperature dependence of free-exciton band intensity had the maximum at ~150 K. The band-A of luminescence, due to defects containing sp^2-hybridizedcarbon bonds, is located in the spectral range 350–650 nm with a maximum at ~440 nm and is characterized by the decay time of 8–19 m sec in the temperature range of 80–300 K. The electron-hole liquid recombination radiation in the diamond was observed at temperatures of <200 K and at peak densities of charge carriers of $\geq(0.3–1.0)\times10^{18}$ cm^{-3}. Condensation of electron-hole liquid implies the displacement of the free-exciton intensity maximum on the temperature dependence to higher temperatures. The critical temperature of electron-hole liquid condensation takes values in the range of 160–220 K. The literature data on the diamond light-emitting devices are discussed.

Keywords: diamond, recombination, electron-hole pair, exciton, electron-hole liquid, electron-hole plasma, photoluminescence, cathodoluminescence, KrCl-laser, light-emitting device

1. Introduction

Recombination radiation in semiconductors appears due to radiative recombination of nonequilibrium charge carriers, which are generated in the processes of photon and high-energy particles absorption, or are injected through the contacts [1]. Usually, recombination luminescence is observed in the spectra of photoluminescence (PL), cathodoluminescence (CL) and electroluminescence (EL).

For simple indirect-gap semiconductors (germanium, silicon, diamond), plasma band recombination of electron-hole pairs (at least at low excitation levels) is not observed in the luminescence spectra. Depending on the defect-impurity composition, temperature and density of nonequilibrium carriers, phonon components of radiative recombination bands of free (FE) and bound (BE) excitons, exciton complexes (EC), the electron-hole liquid (EHL) and electron-hole plasma (EHP) are observed in the luminescence spectra of the sample near the fundamental absorption edge. In the latter case, there is a bound state of nonequilibrium charge carriers arising when the Mott transition is fulfilled (phase transition of the second kind)—transition gas FE–EHP. In addition to the processes mentioned above, the radiative recombination of nonequilibrium charge carriers can occur through the impurity-defect allowed states located in the band gap. In this case, recombination emission bands are observed in the spectral region close to the half-width of the energy gap.

Due to the short covalent C–C bond, the low dielectric constant and high Debye temperature diamond excel other semiconductors. **Table 1** shows comparative data on diamond and other semiconductor-related recombination radiation.

Semiconductor	**Electric constant, ε**	**Debye temperature, T [K]**	**Binding energy of free exciton, E_x [meV]**	**Radius of free exciton, a_x [nm]**	**Critical EHL carrier density, n [cm^{-3}]**	**Critical EHL temperature, T [K]**
Germanium, Ge	15.6	374	3.2	15.37	8.9×10^{16}	6.7
Silicon, Si	11.4	640	14.3	4.15	1.2×10^{18}	28
Silicon carbide, 3C-SiC	9.7	1200	13.5	3	2.3×10^{18}	41
Gallium phosphide, GaP	9.1	445	10	5	2.6×10^{18}	45
Diamond, C	5.7	1860	80.5	1.26	3×10^{19}	>165

Table 1. Characteristics of some indirect-gap semiconductors associated with the recombination radiation: electric constant, Debye temperature, the binding energy of exciton, the free-exciton radius, critical temperature, and concentration for formation of EHL.

Diamond is characterized by high exciton binding energy (80.5 meV) [2], which corresponds to a temperature of 660°C. At room temperature, the thermal energy of the charge carriers is

less than twice the binding energy of FE. At the temperature of liquid nitrogen, binding energy of FE in the diamond exceeds the thermal energy of lattice on an order of magnitude. Therefore, nonequilibrium charge carriers in diamond form FEs, because it is energetically favorable for them. These temperatures are not extremely low (helium). At the same time, the high density of trapping/recombination centers of charge carriers hinders the formation of FE. However, in the diamond samples containing the impurity-defect centers of $<10^{18}$ cm^{-3}, nonequilibrium charge carriers being generated or injected (at small values of the electric field) form excitons, which are then involved in the radiative and nonradiative recombination, the formation of the EC, condensation and evaporation of EHL.

This chapter of the book is devoted to the review process of radiative recombination FE, EHL, and EHP bands, as well as the so-called band-A of luminescence. We discuss the observed effects, the outstanding issues and possible research directions.

2. Experimental

We investigated the properties of several diamond samples, whose main characteristics are given in **Table 2**.

Sign	Synthesis method	Monocrystal/ polycrystalline	Size [mm]	Transparency	FE-band	Band-A	EHL-band
C4	Natural	Mono	∅4 × 0.25	Yes	No	Strong	No
C5	Chemical vapor deposition (CVD)	Poly	10 × 10 × 0.5	Yes	Strong	Very weak	Strong
C6 (fragments)	CVD	Poly	10 × 10 × 0.1	Yes	Weak	Very weak	No
C10	CVD	Mono	5 × 5 × 0.25	Yes	Strong	No	Strong
C11	CVD	Poly	5 × 5 × 0.25	No	No	Very weak	No
C12	High-pressure high-temperature (HPHT)	Mono	5 × 5 × 0.25	Yes	Strong	No	Weak

Table 2. General characteristics of diamond samples: synthesis method, monocrystal/polycrystalline, size, transparency, observation of spectral FE-, band-A, or EHL-components.

The densities of impurities and defects in samples were less than 10^{18} cm^{-3}. IR absorption spectra of samples did not reveal any peculiarities in one-phonon absorption in the range of 7.5–15 microns (see Ref. [3]), due to the impurity-defect centers.

IR absorption spectra were measured at room temperature (RT) using infrared spectrometer Nicolet 5700 with Fourier transformation in the spectral region from 2.5 to 15 microns. Raman spectra of samples in the wave number range of 100–3700 cm^{-1} were obtained at RT using the

same infrared spectrometer equipped with the Raman attachment NXR FT-Raman. Spectral resolution was 2 cm^{-1}.

The PL spectra of diamond samples were measured at temperatures from 80 to 300 K using spectrometer Ocean Optics HR 4000 in the spectral range of 200–300 nm with spectral resolution of 0.4 nm and Stellar-Net EPP-2000C in the spectral range of 200–850 nm with resolution of 1.5 nm. Before measurements, diamond sample was mounted on a cooled copper holder, placed in a vacuum chamber. The sample temperature was measured with a platinum thermoresistor Heraeus Pt1000. Excitation of PL was provided by pulsed KrCl-laser radiation (λ = 222 nm) with pulse duration 18 ns (FWHM) or ArF-laser radiation (λ = 193 nm) with pulse duration of 8 ns (FWHM). Laser pulse energy was 30 mJ. The radiation was focused on a sample by a quartz cylindrical lens with a focal length of 65 mm. The peak intensity of the laser radiation on the surface of the sample reached 13 and 10 MW/cm^2 at 222 and 193 nm, respectively. PL radiation from the opposite side of the diamond sample (excitation relative) was transported to the spectrometer through the optical fiber. The incident energy on the sample was measured by laser radiation pyroelectric sensor Ophir PE50-BB. The experimental scheme is described in detail in Ref. [3].

Figure 1 shows the evacuated chamber design, which was used to research the pulse PL of diamond samples at cooling from room temperature (RT) to the temperature of liquid nitrogen. The design of this camera also enables to conduct the measurement of diamond photoconductivity.

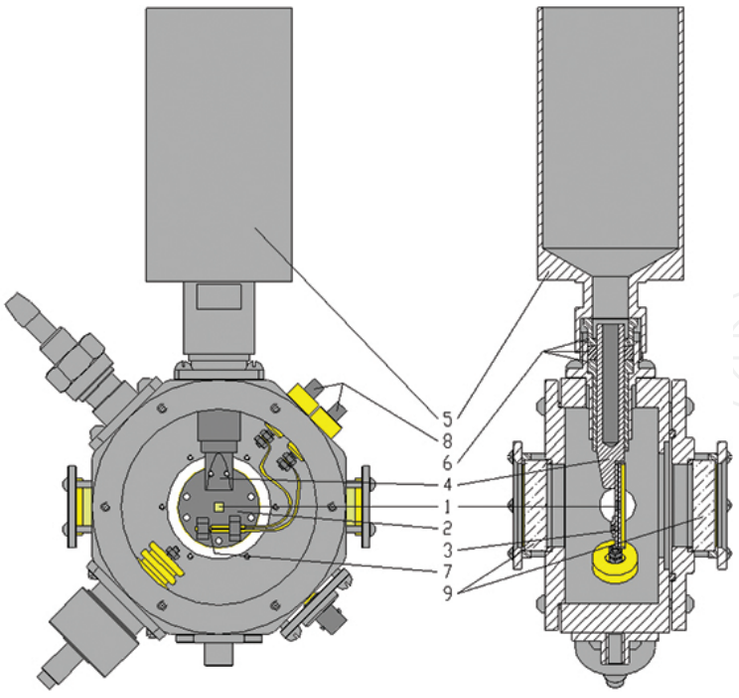

Figure 1. Vacuum chamber. **1**-diamond sample; **2**, **3**-copper round plates; **4**-hollow copper heat sink; **5**-metal cup with liquid nitrogen; **6**-seals; **7**-platinum thermistor; **8**-vacuum-tight electrical bushings; **9**-fused silica windows.

http://dx.doi.org/10.5772/65064

Diamond sample **1** was placed between two copper round plates **2** and **3**. In the center of each plate, there was a square hole 3 × 3 mm^2. Plates were fastened to the hollow copper heat sink **4**. The heat sink **4** was out of the evacuated chamber in a metal cup **5** with liquid nitrogen. The vacuum seal and partial heat insulation were provided with seals **6** (polyamide, vacuum rubber). To measure sample temperature, the platinum thermistor **7** (Heraeus Pt1000) has been placed on the copper plate **2** in contact in the copper holder. The resistance of the thermistor **7** was measured with a multimeter (MY-64 S-line) through vacuum-tight electrical bushings **8**. The temperature of the diamond sample **1** was considered equal to the temperature of the thermistor **7** and was determined from the temperature dependence of thermistor resistance provided from the device data sheet. In the experiment, the temperature range of the thermistor resistance decreases from 1100 to 225 ohms. Thus, the minimum temperature recorded was 80 K at a fore-vacuum pump (~10^{-2} torr).

Thermal contact of the sample **1**, copper plates **2** and **3**, heat sink **4** and the thermistor **7** was provided by thermopaste KPT-8 with a specific electrical resistance >10^{12} Om cm. The laser beam fell into the sample through a quartz window **9**. The chamber pumping was made by the backing pump 2NVR-5DM.

The absorption of photons in the diamond sample leads to a nonuniform distribution of nonequilibrium charge carriers. Reduction in the peak intensity of the laser radiation with the depth of the sample (taking into account the reflections from the rear face) is calculated by the formula [4]:

$$I(x) = I_0 \cdot \frac{(1-r)\cdot\left(e^{-\alpha\cdot x} - r\cdot e^{-\alpha\cdot(2\cdot d - x)}\right)}{1 - r^2\cdot e^{-2\cdot\alpha\cdot d}} \quad (1)$$

where x [cm]—depth, I_0 [W/cm^2]—the peak intensity of the laser radiation on the surface of the sample, r—reflection coefficient of diamond at the laser wavelength (r_{222} = 0.21031, r_{193} = 0.24432 [5]), α [cm^{-1}]—the absorption coefficient of the sample at the laser wavelength (α_{222} = 400 and α_{193} = 3250 cm^{-1}), d [cm]—thickness of the sample.

Profiles of charge carrier peak density over the sample thickness were calculated using the formula [6]:

$$n(x) = \frac{I(x)\cdot\tau}{h\nu\cdot x} \quad (2)$$

where $I(x)$ [W/cm^2]—profile of the laser radiation peak intensity with the depth of the sample, calculated according to the formula (1), τ [s]—lifetime of nonequilibrium charge carriers, $h\nu$ [J]—the energy of photons.

Figure 2 shows the distribution of the laser peak intensity and the peak carrier density in the sample, calculated by the formulas (1) and (2), at peak laser intensity I_{222} = 13 MW/cm^2 and I_{193} = 10 MW/cm^2.

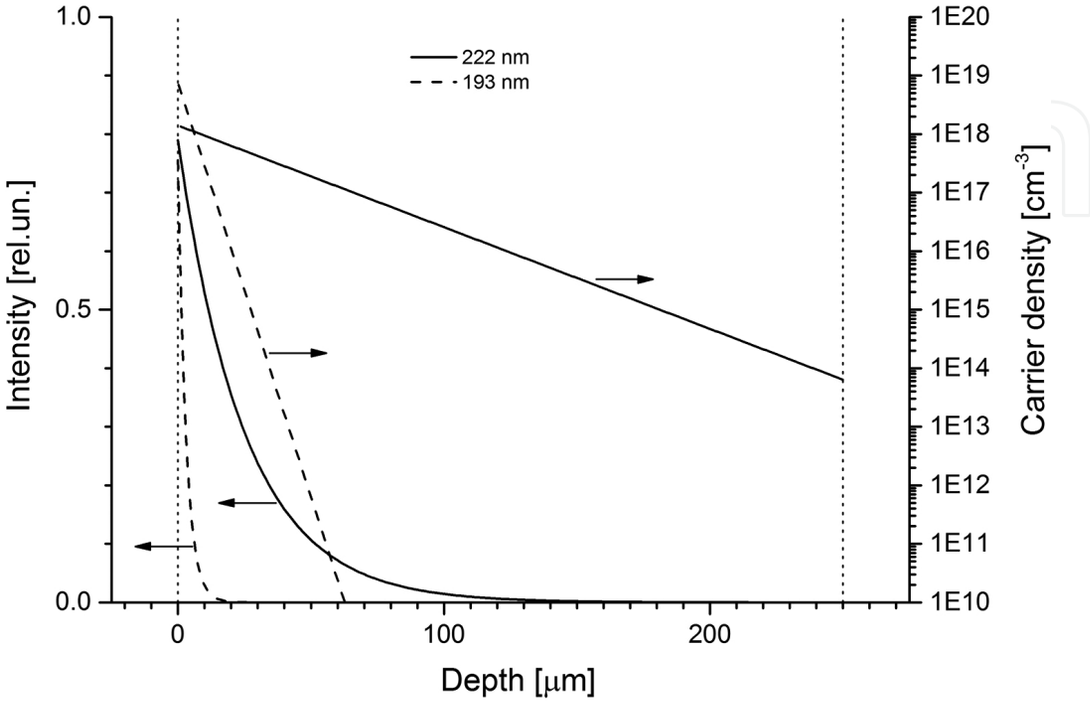

Figure 2. Laser intensity and charge carrier density in the diamond sample C5 versus the depth of sample for laser excitation on 222 nm (solid curves) and 193 nm (dashed curves).

Thus, the photons at 222 and 193 nm created in the samples the maximum nonequilibrium charge carrier density of $n_{222} \sim 1.1\times10^{17}$ and $n_{193} \sim 5.6\times10^{17}$ cm^{-3}, respectively. The carrier density reduced exponentially by two orders of magnitude in the diamond layer thickness $d_{222} \sim 110$ microns and $d_{193} \sim 13$ microns, respectively.

CL spectra were measured using another vacuum chamber, a similar device. The camera was attached directly to the electron accelerator. The luminescence radiation of a sample was transported to a spectrometer through the optical fiber. The technique of CL measurements is described more detailed in [7].

3. Free exciton recombination band

In the diamonds with the densities of impurity-defect centers of less than 10^{18} cm^{-3}, the recombination FE band is characterized by considerable intensity even at RT. In Ref. [8], observation of the FE luminescence band of the diamond sample doped with boron at temperatures up to 277°C was reported. Presumably, in luminescence spectra of undoped ultrapure samples, the FE recombination band can be observed up to temperatures of ~660°C.

http://dx.doi.org/10.5772/65064

Due to the indirect zone structure in the diamond, the FE radiative recombination arises with the generation of momentum-conserving phonons. Recombination radiation of FEs in diamond is accompanied by the generation of the three main phonon components—the dominant TO (transverse optical phonon 141 meV) at 5.275 eV, TA (transverse acoustic phonon 87 meV) at 5.325 eV and TO+O^{Γ} (two-phonon process involving TO + Raman phonon 141 + 159 meV) at 5.117 eV, as shown in **Figure 3**. The LO-component (longitudinal optical phonon 156 meV) at 5.254 eV is characterized by low intensity and is indistinguishable on the background of intense temperature-broadened TO-components at temperatures higher than 100 K [9].

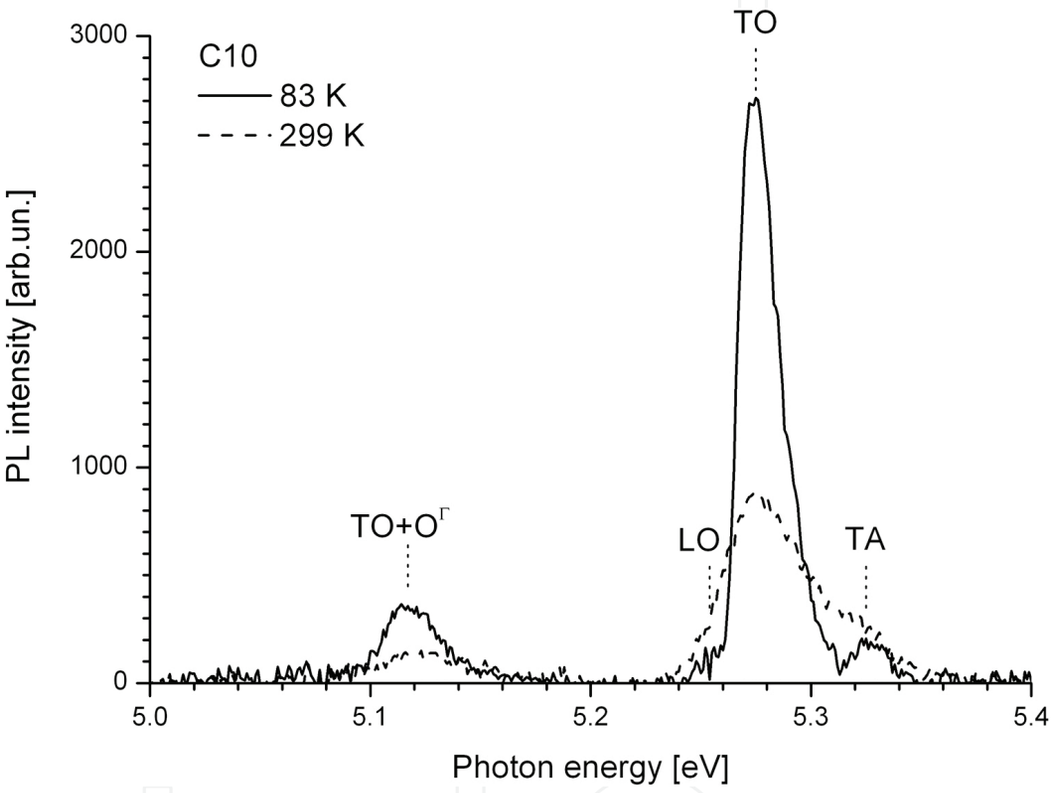

Figure 3. PL integrated spectra of diamond monocrystal C10 under excitation at 222 nm at temperatures of 83 K (solid curve) and 299 K (dashed curve). The spectrum contains the phonon components: TA (87 meV) at 5.325 eV, TO (141 meV) at 5.275 eV, LO (156 meV) at 5.254 eV and TO + O^{Γ} (141 + 159 meV) at 5.117 eV.

The spectral position of the phonon component of the recombination FE band $h\nu$ was determined by the band gap E_g, the binding energy of FE E_{FE}, and the corresponding phonon energy $h\omega$:

$$h\nu = E_g - E_{FE} - h\omega \tag{3}$$

Depending on experimental conditions, all three terms in the right side of the expression (3) vary slightly, causing the displacement of the spectral components.

It is known that the band gap decreases with increasing temperature due to increase in thermal energy of the atomic lattice [10]. In Ref. [11], the difference between the band gap E_g and exciton binding energy E_x in the 80–620 K temperature range was measured by finding the position of the phonon component of exciton absorption threshold at 5.258 and 5.314 eV for several natural diamonds. In the temperature range 80–300 K, the reduction of value $E_g - E_x$ was ~15 meV (see. **Figure 4**). According to Eq. (3), this reduction, $E_g - E_x$, should cause a corresponding shift of the maxima of phonon FE component. In Ref. [12], the position of TO-component maximum of FE recombination was measured in the temperature range 80–250 K for CVD diamond samples (see **Figure 4**). The FE band maximum shifted to shorter wavelengths by ~16 meV as the temperature increases from 80 to 200 K. This observation contradicts to the effect of band gap reduction with increasing temperature.

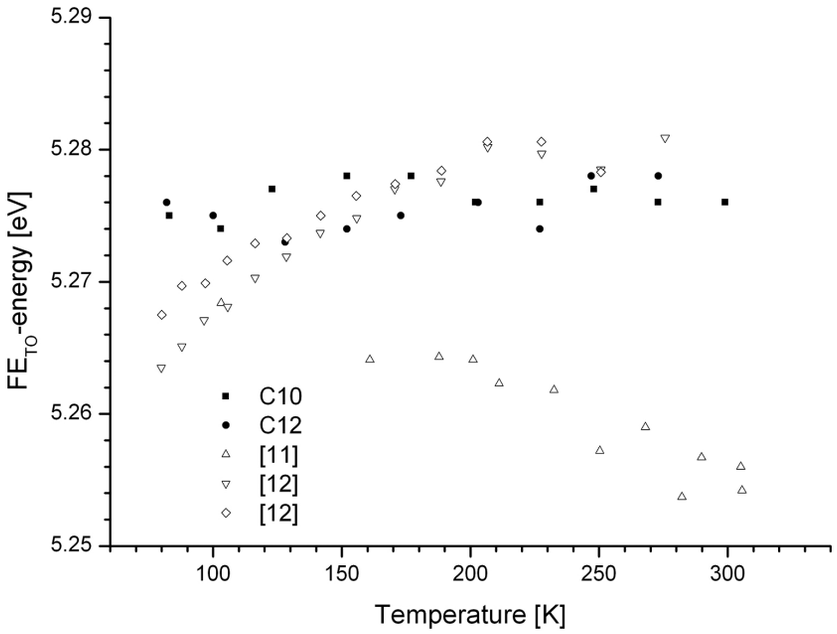

Figure 4. Positions of indirect optical transitions depending on diamond sample temperature. Excitation was provided at 222 nm with peak intensity 1 MW/cm^2. Black squares-sample C10, black circles-sample C12, open triangles-data from Ref. [11], open turned triangles and open rhombs-data from Ref. [12].

We have measured the position of dominant TO-component maximum of FE recombination depending on the temperature for the samples C10 and C12 at low level of excitation at 222 nm. The measured values are shown in **Figure 4**. The observed change in the maximum position of radiative FE recombination is about 3–5 meV, which lies within the measurement error, and is significantly less than one measured in [11]. In Ref. [12], there was another trend of TO-component position shifting to shorter wavelengths with increasing temperature. Thus, the data are inconsistent, and the observed phenomena deserve separate studies.

At low excitation levels, the binding energy of FE in diamond is 80.5 meV [2]. As the FE density approaching the Mott transition level or EHL condensation critical density (phase transition of the first kind), which is characterized by a decrease in the average distance between FEs to

a value r_s = 1–2 (in FE radius size), the FE binding energy should decrease to zero [13]. In the literature, there is no information for diamonds about the FE binding energy measurements under such conditions.

For various diamond samples with various defect-impurity compositions, different phonon energy is mentioned for indirect optical transitions of radiative recombination. **Table 3** shows the values of TA-, TO-, LO- and O^{Γ}-phonon energies to various literature references.

References	Phonon energy, meV			
	TA	**TO**	**LO**	**O^{Γ}**
[11]	83	143	132	167
[2]	83.6	135.8	156	159.2
[9]	87	141	163	165
[14]	87	140	–	151
[15]	88	140	162.4	164.2

Table 3. Energies of TA-, TO-, LO- and O^{Γ}-phonons from a variety of published data.

Differences in phonon energies arise from different calculation methods, measurement errors and experimental conditions. Experimental conditions are the most important thing, because it is necessary to use the phonon energy as the varying values for the best fit of the experimental and calculated data. This indicates an incomplete understanding of observed phenomena.

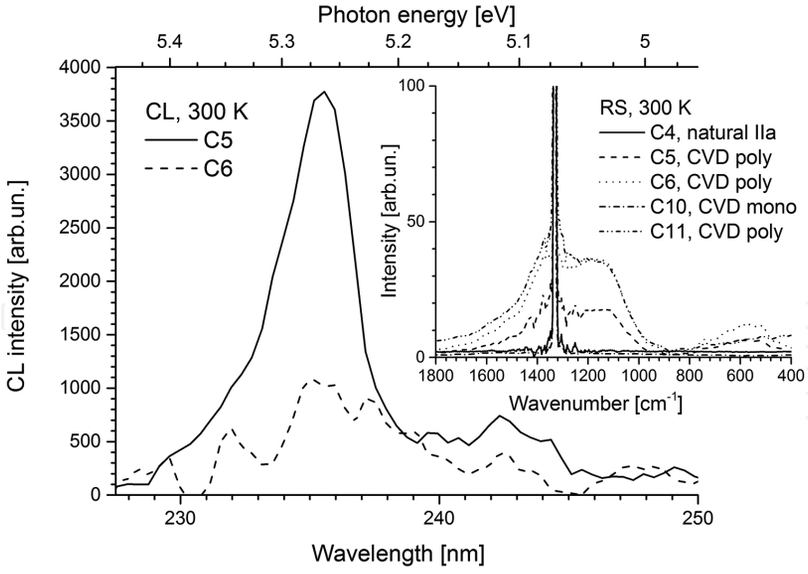

Figure 5. CL integrated spectra of polycrystalline CVD diamond samples C5 and C6 at room temperature. The CL excitation was provided by high-current electron beam (220 keV) with pulse duration of 2 ns. On the inset Raman spectra of several diamond samples at room temperature are shown.

The presence of defects and impurities in the sample increases the probability of nonradiative recombination processes of FEs. CL spectra at room temperature of two different polycrystal-

line CVD diamond samples C5 and C6 are shown in **Figure 5**. FE recombination band dominated in both spectra. The inset in **Figure 5** shows the Raman spectra of several diamond samples, including C5 and C6. For comparison, the spectra of natural (C4) and CVD single crystals (C10), as well as a fully opaque CVD polycrystalline sample (C11), are presented. In contrast to sample C5, the Raman spectrum of sample C6 is characterized by high intensity "non-diamond" bands: amorphous carbon (570–580 and 1540 cm^{-1}), disoriented graphite (1350 cm^{-1}) and microcrystalline diamond (1140 cm^{-1}). These features are reflected in the intensity of FE band. Thus, the presence of large density of states of "non-diamond" carbon increases the probability of nonradiative recombination and reduces the probability of optical transitions in FE band. Samples C5 and C6—diamonds of "optical quality"— had no measurable absorption bands in the IR range, had low intensity of luminescence band-A (see Section 4), showed no other luminescence bands (except the band-A and the FE band) and revealed the clear edge of fundamental absorption [3]. In addition, sample C5 demonstrated the radiative recombination of EHL at higher excitation levels [3, 16], which will be discussed in Section 5.

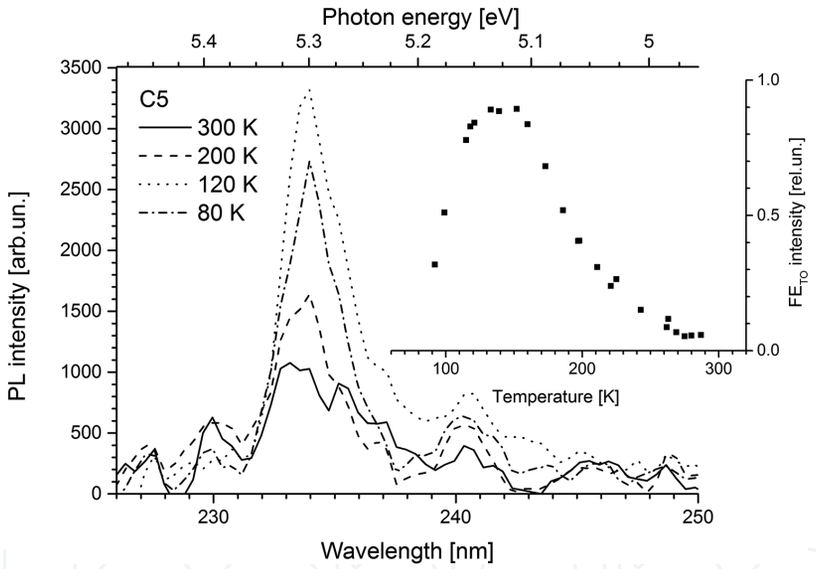

Figure 6. PL integrated spectra of polycrystalline CVD diamond sample C5 at different temperatures. The PL excitation was provided by KrCl-laser (222 nm) with pulse duration of 18 ns. On the inset there is the temperature dependence of FE band intensity of diamond sample C5.

The intensity of FE recombination band varies with the temperature of the sample as shown in **Figure 6**. At low excitation levels, this dependence has the form as shown in the inset of **Figure 6** and is determined by the FE lifetime of charge carriers in diamond [17]:

$$\frac{1}{\tau_{FE}} = P_{FE} + F_{FE} \cdot \exp\left(-\frac{E_{FE}}{kT}\right) + R_T \cdot \frac{P_{BE}}{P_{BE} + F_{FE} \cdot \exp\left(-\frac{E_{FE}}{kT}\right)} \quad (4)$$

where P_{FE}—annihilation rate FE, the second term—the rate of FE thermal ionization with frequency F_{FE} and binding energy E_{FE}, the third term—the localization rate of bound excitons (BE) on shallow traps, R_T—capture speed of FE, R_{BE}—the BE annihilation rate, F_{BE}—frequency of BE thermal dissociation on a FE and a trap, E_{BE}—binding energy of BE.

The intensity maximum of TO-component of recombination FE band usually locates at temperature about 150 K for all diamond samples and excitation methods [12, 17, 18]. The exception is the PL at high excitation levels (see Section 5).

Thus, the FE recombination radiation in the diamond at low excitation levels has been studied quite well. However, there are following unresolved aspects: the absence of spectral shifting of dominant TO-component, when the temperature changes; the different phonon energies of FE recombination component in different experiments; and the unknown change in FE binding energy by increasing the charge density to values $\geq 10^{19}$ cm^{-3}.

4. The band-A of luminescence

Diamond samples of any synthesis method show the blue luminescence band (350–650 nm) in the visible region of luminescence spectra. This so-called band-A is observed at any excitation method [19] (See **Figures 7–9**). There is a competition between the FE recombination band and band-A [8]. More defective samples show intense band-A, and purer samples—intensive FE band. Thus, the centers of band-A are effective FE radiative recombination centers.

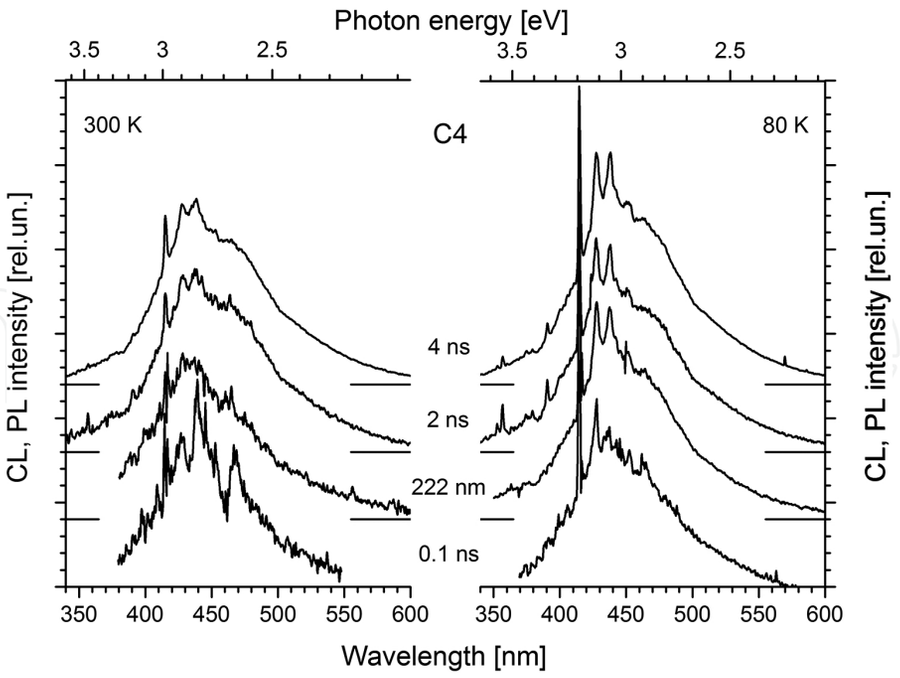

Figure 7. CL and PL integrated spectra of natural diamond IIa-type sample C4 at temperatures of 300 and 80 K. The CL excitation was provided by electron beams with durations of 0.1, 2, and 4 ns. The PL excitation was provided by KrCl-laser with pulse duration of 18 ns.

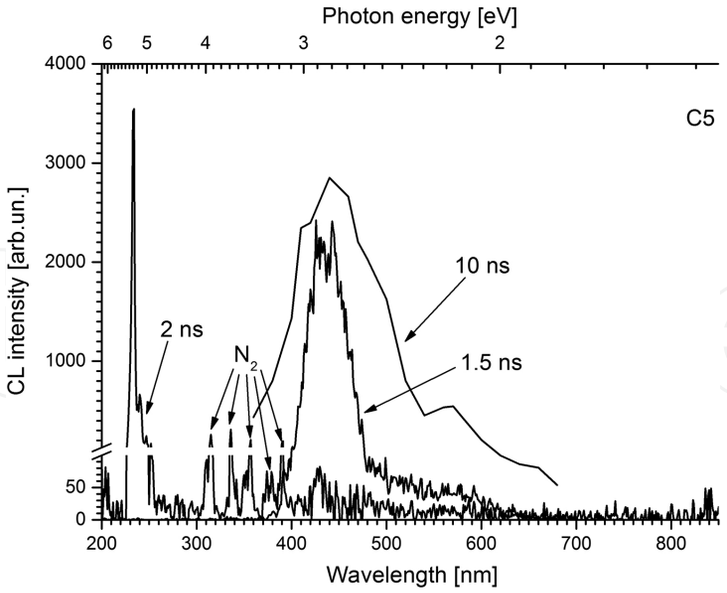

Figure 8. CL integrated spectra of polycrystalline CVD diamond sample C5 at room temperature. The CL excitation was provided by several electron beams with pulse duration of 1.5, 2, and 10 ns. The integrated spectrum obtained at 1.5 ns excitation was magnified in 30 times compared with the spectrum obtained at 2 ns excitation. The spectrum obtained at 10 ns excitation was reconstructed from the maximum of CL emission signals at different wavelength (the method see in Ref. [29]) and was normalized to intensity of CL spectrum obtained at 1.5 ns excitation.

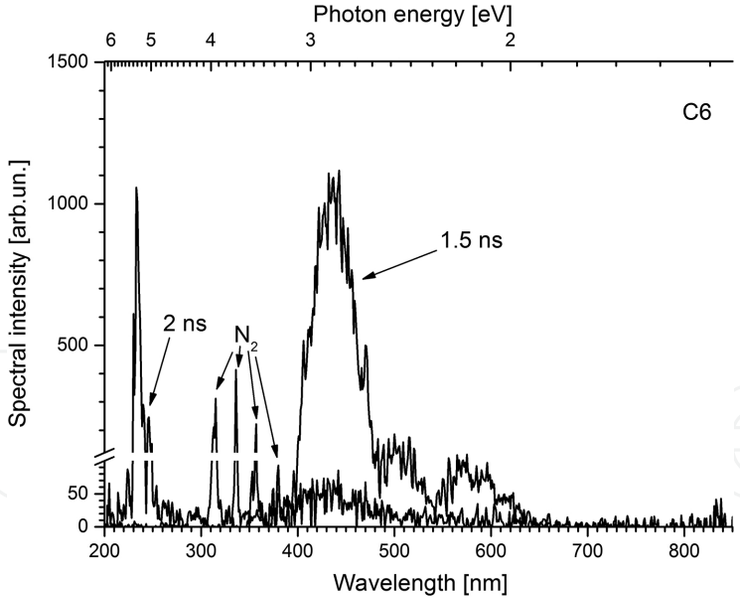

Figure 9. CL integrated spectra of polycrystalline CVD diamond sample C6 at room temperature. The CL excitation was provided by electron beams with pulse duration of 1.5 and 2 ns. The integrated spectrum obtained at 1.5 ns excitation was magnified in 30 times compared with the spectrum obtained at 2 ns excitation.

There is no common opinion about the origin of luminescence band-A. Initially, luminescence analysis objects of the diamond structure were natural crystals and specimens grown in conditions of high pressure and high temperature (HPHT). Such samples always contain

nitrogen in significant densities (10^{17}–10^{20} cm^{-3}) in the dispersed form or in polyatomic complexes. In Ref. [20], it was suggested that the band-A is the result of recombination of electrons and holes on closely spaced donor-acceptor pairs. However, intensive band-A was observed in samples containing impurities below 10^{17} cm^{-3} [21]. In [19], band-A has been attributed to optical transitions in N_4V centers. However, a clear correlation between the intensities of the band-A and N9 system (associated with N_4V centers) has not been identified [22]. In Refs. [8, 12, 23, 24], it has been proposed that band-A is associated with dislocations. However, not all of the dislocations were luminesced [19, 23], a clear correlation with the type of dislocation was not observed [25], and band-A radiation may come from sample areas, which are free from dislocations [23]. Sometimes, the observed emission of band-A appeared from a single dislocation, which has led to assume about the optical transitions in defect centers, decorating dislocation and dangling bonds in dislocations.

The development of CVD technology was enabled to receive diamond samples of large sizes (up to Ø120 × 3 mm^3) [26]. Untreated CVD diamonds contain no nitrogen with aggregation degree of more than 2, because the synthesis gas receives nitrogen from air only. The observation of band-A in luminescence spectra of undoped CVD diamonds has led to speculation that the band-A is a result of recombination of electron-hole pairs on lattice defects, containing the sp^2-hybridized carbon bonds [27]. In natural diamonds subjected to natural HPHT treatment, this type of defects exists throughout the whole volume of sample [19].

The band-A is practically immeasurable in CVD single crystals [3]. Intrinsic defects, containing sp^2-hybridized carbon bonds, are concentrated in grain boundaries of polycrystalline CVD diamonds [28]. In Ref. [21], it was found that the band-A of CVD polycrystalline diamond luminescence is observed from defective disoriented areas—grain boundaries. Calculations [28] showed that the grain boundaries contain ~40% of amorphous carbon with sp^3-hybridized carbon bonds, preserving the short-range order of diamond lattice only, ~10% of dangling bonds and ~30% of sp^2-hybridized carbon dimers, which create allowed states in the band gap. The radiative recombination of FEs in the spectral region of band-A occurs through allowed states in the band gap.

In Ref. [8], there was competition between the FE recombination band and band-A in the CVD diamond films. The increase in boron impurity density led to the emergence of "non-diamond" bands in Raman spectra, reduction of FE band intensity and increase in the band-A intensity and vice versa. The FE binding energy in the diamond is about two times higher than heat energy at room temperature. There is a competition between the processes of spontaneous FE radiative recombination and FEs capture on band-A defects.

Natural samples (e.g., C4), containing a small amount of N_2 defects, exhibit intensive band-A of luminescence in the spectral range of 350–650 nm (see **Figure 7**). The luminescence spectra of polycrystalline CVD samples of "optical quality" contain the dominant FE recombination band at 235.2 nm. At the same time, the band-A is characterized by low intensity (see **Figures 8** and **9**).

The natural diamonds and synthetic samples, which were subjected to HPHT treatment, demonstrate the band-A of luminescence that overlapped the bands of other defects [22]. These

defects (N_3V, N_2V and NV centers) show vibronic bands of luminescence with the zero-phonon lines (ZPL) at 415, 503 and 575 nm, respectively. For this reason, the integrated luminescence spectra of the diamonds in the visible region can have multiple peaks and exhibit shifts from sample to sample. **Figure 7** shows the CL and PL spectra of the natural type IIa specimen (C4). CL was excited by electron beam with pulse duration of 0.1, 2 and 4 ns; for PL excitation, the pulsed laser radiation at 222 nm with a pulse duration of 18 ns (FWHM) was used. Besides band-A, the luminescence spectra exhibit the so-called N3 system with ZPL at 415.2 nm due to N_3V centers.

Measurements of luminescence spectra with time resolution allow to resolve the band-A and superimposed bands in time. **Figure 10** shows the change in the CL spectrum of natural sample C4 in time. The CL spectrum in the maximum of optical signal consisted of system N3 with ZFL 415.2 nm and its phonon replicas (427, 438, 450 and 463 nm), and the wide anti-Stokes (with respect to the ZPL) component at 350–410 nm. At 30 ns after starting of excitation pulse, the CL intensity decreased by seven times, the position of the ZPL and phonon replicas did not change, and anti-Stokes luminescence component drastically decreased. At 2 ms after starting of excitation pulse, the ZPL 415.2 nm and its phonon replicas completely disappeared, and the intensity was reduced by three orders of magnitude, maximum shifted to 450–480 nm.

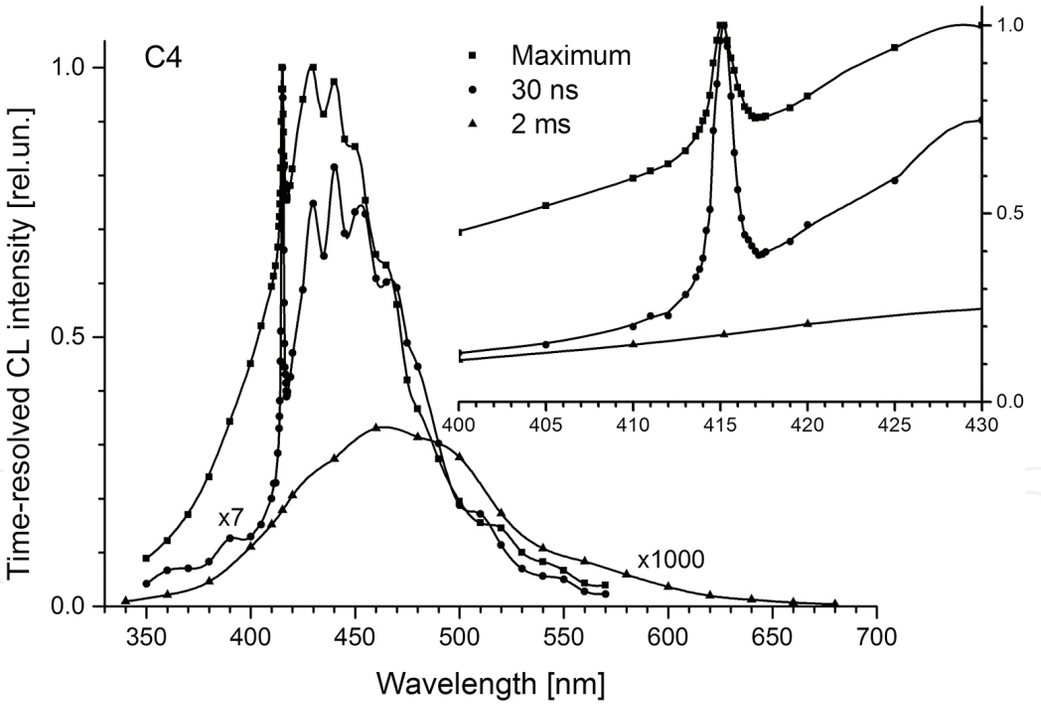

Figure 10. CL spectra of natural diamond sample C4 at room temperature obtained at 10 ns excitation. CL spectra were reconstructed at different wavelength (the method see in Ref. [29]) from the maximum of CL emission signals (squares), after 30 ns from the excitation starting (circles) and after 2 ms from the excitation starting (triangles). On the inset, there are CL spectra in the magnified spectral scale.

Thus, the band-A is characterized by prolonged weak emission in the 350–650 nm range with decay time 8–9 ms at room temperature, as shown in **Figure 11**. At temperature ~80 K of

diamond sample, the decay time increased up to 18–19 ms [7, 29]. The temperature dependence of the band-A was investigated in detail earlier [23]. The sample heating from 30 to 110°C resulted in complete quenching of the band-A. In Ref. [22], the observation of band-A at temperatures up to 125°C was reported. So the activation energy of nonradiative recombination of band-A centers is about 35 meV.

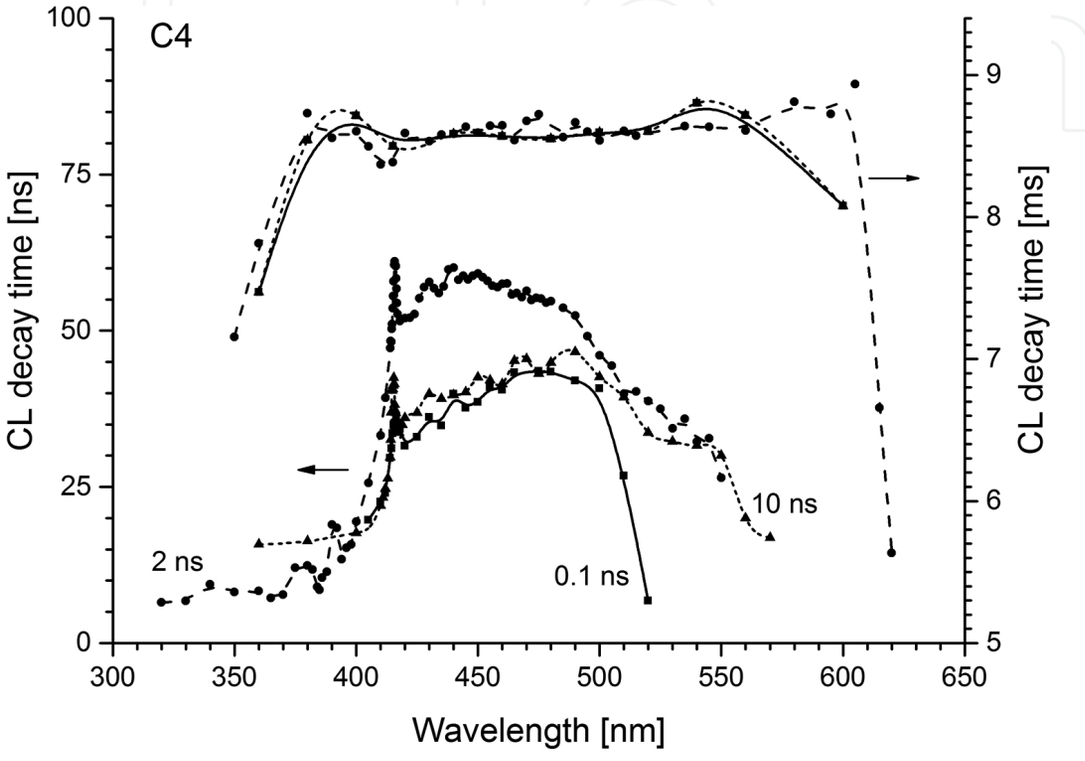

Figure 11. Spectra of CL decay time of natural diamond sample C4 at room temperature in nanosecond and millisecond time scale. The vibronic N3 system (N_3V centers) is characterized by the nanosecond decay time of CL. The band-A (sp^2-hybridized bonds) is characterized by the millisecond decay time of CL. Note that the CL decay time spectrum of band-A did not changed at different durations of electron beams and was 8–9 ms in the whole emission range. Squares-e-beam pulse duration of 0.1 ns, circles-2 ns, triangles-10 ns.

The observed temperature quenching of band-A in nonradiative recombination processes showed the complex structure of energy levels of corresponding defects. Temperature quenching was observed at temperatures above 80 K. There are no references in the available literature about the dependence of band-A intensity at temperature less than 80 K.

Thus, the experimental data indicate that the recombination band-A of luminescence in the diamond is due to the intrinsic defects of the diamond lattice, containing the sp^2-hybridized carbon bonds. The lifetime of the metastable excited level centers of band-A is ~8–19 ms in the temperature range 300–80 K. The activation energy of temperature quenching of band-A is ≥35 meV. At the same time, the atomic structure and the position of energy levels of band-A centers are not known exactly. Research in this area will improve the understanding of defect formation in diamond and advance in the synthesis of ultra-pure diamond samples for optoelectronic applications.

5. Electron-hole liquid recombination band

The electron-hole liquid (EHL) is a condensed state of FE gas in semiconductors [13]. For the condensation of EHL, it is necessary to provide the temperature below the critical point and high charge carrier density. The EHL exists in the form of droplets with size 10^{-8}–10^{-4} m depending on the material. The lifetime of the EHL is determined by the charge carrier lifetime and the processes of droplet condensation/evaporation. The EHL is observed in PL and CL spectra in the form of recombination band shifted toward longer wavelengths relative to FE recombination band.

EHL properties in germanium and silicon are well understood [30]. For them, the critical constitute 6.7 K and 24.5 K, respectively. Diamond is the third one-component indirect-gap semiconductor. Due to the high FE binding energy of 80.5 meV and the high Debye temperature of 1860 K, the critical temperature of EHL existence in diamond is more than 160 K [31–33].

The first reports on the EHL observation in diamond have been made quite recently [33, 34] as improving CVD synthesis technology. Observation of EHL in luminescence spectra of natural diamonds (as well as FEs) is difficult because of high level of doping with nitrogen [31]. These defect centers act as nonradiative (N_S, N_2, N_4V) and radiative (N_3V, N_2V, NV, sp^2-bonds) centers of FE recombination. Currently, the EHL properties in diamond attract some interest [3, 35].

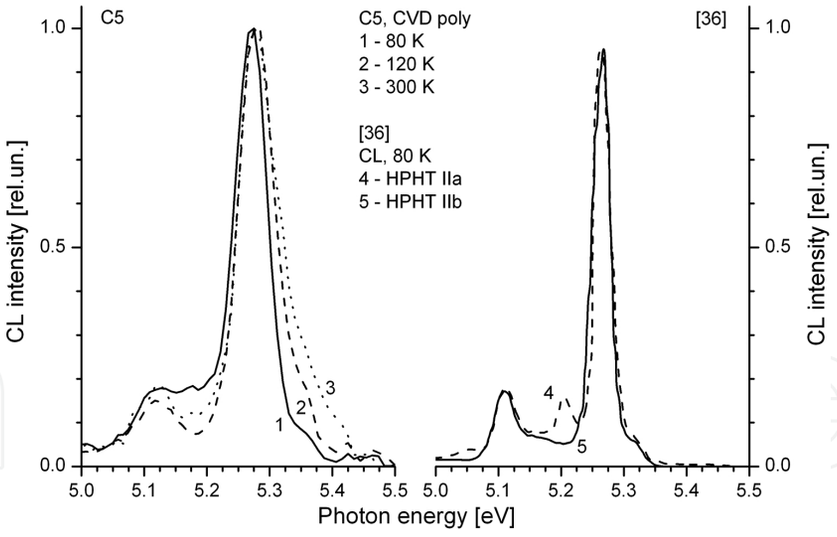

Figure 12. CL spectra of polycrystalline CVD diamond sample C5 at several temperatures from 80 up to 300 K at excitation by 2-ns electron beam (left part). CL spectra of two HPHT samples at 80 K from Ref. [36].

The observation of EHL recombination band in CL spectra of the diamond is complicated by heating the area of electron beam exposure. An accelerated electron generates tens-thousands of "hot" electron-hole pairs, which then thermalize in cascades of phonon emission, causing the heating of lattice and the "phonon wind," making difficulties to EHL condensation. In CL spectra, the EHL recombination band is observed in the form of low-intensity band at 5.16–

http://dx.doi.org/10.5772/65064

5.23 eV range and between TO- and TO+O^{Γ}-components of FE recombination band (see **Figure 12**, CVD sample C5). In addition to this work in the available literature, it was reported only once about the EHL recombination band in CL spectra of the HPHT IIa type (pure) and IIb type (doped with boron) diamonds [36].

The excitation of nonequilibrium charge carriers by laser radiation provides less heating of the lattice, as an absorbed photon produces an electron-hole pair. Moreover, if the excitation of nonequilibrium carriers by laser radiation takes place at the fundamental absorption edge, the generated carriers will have a minimum excess energy, and consequently, less laser energy is converted to the lattice heating and the "phonon wind."

The threshold laser intensity for the observation of EHL recombination band in the PL spectra depends on the fundamental properties of the material, as well as the impurity-defective composition of a particular sample. The higher the recombination center density in the sample is, the higher the threshold intensity to compensate the exciton recombination should be. On the other hand, some impurity-defect centers can act as condensation nuclei of EHL drops, which should reduce the threshold intensity, as condensation on the irregularities is thermodynamically favorable than the condensation in the homogeneous vapor [13, 37].

Figure 13 shows the PL spectra of polycrystalline diamond sample C5 in the temperature range 90–235 K with excitation at 222 nm with peak intensity of 3 MW/cm² [38]. The EHL recombination band is observed in the form of long-wavelength shoulder (5.2–5.16 eV) of TO-component of FE band. The EHL recombination radiation arises from the central regions of crystallites, but not from the crystallite boundaries. **Figure 14** shows a micrograph of sample C5 with magnification ×4. Crystallite sizes range from 50 to 400 microns, which is significantly higher than the FE diffusion length in diamond (1–10 microns) at RT [21, 39, 40].

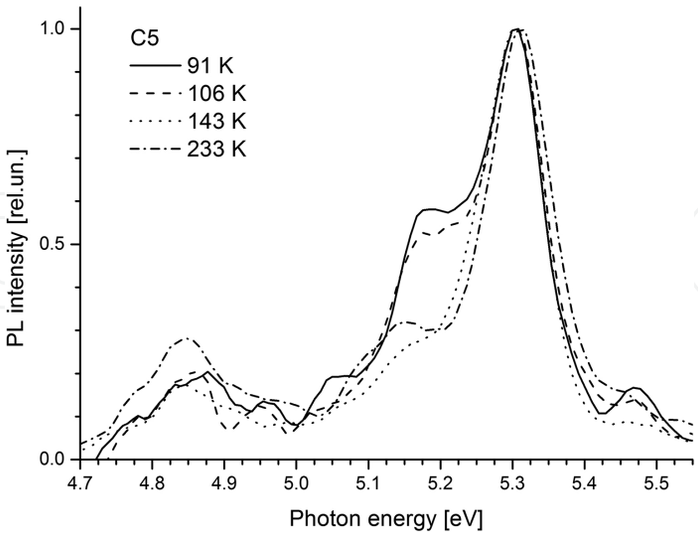

Figure 13. PL spectra of polycrystalline CVD diamond sample C5 at several temperatures from 80 K up to 300 K at excitation by 18-ns laser pulses at 222 nm with peak intensity 3 MW/cm². The TO-component of FE band at 5.27 eV dominated in PL spectra. The TO-component of EHL band in the spectral range 5.1–5.2 eV was appeared on the long-wavelength edge of FE band.

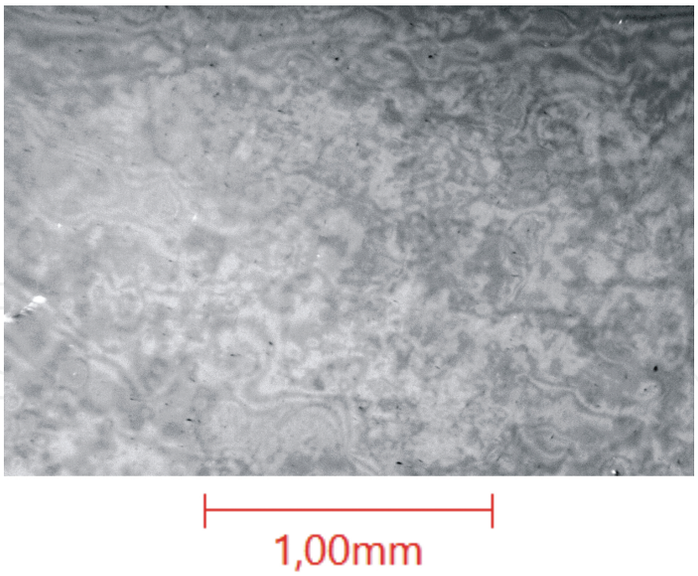

Figure 14. The microphotograph of surface of polycrystalline CVD diamond sample C5 with magnification ×4. The crystallite sizes take values from 50 up to 400 μm.

For a single-crystal sample C10 with excitation at 222 nm, the threshold intensity of EHL recombination band was about 7 MW/cm^2, which is more than two times higher than the threshold intensity for sample C5. The reason for this effect has not yet been established.

In addition to changing the threshold intensity for observation EHL recombination radiation from sample to sample due to its different impurity-defective structure, the threshold intensity also depends on the excitation wavelength. As mentioned above, the higher photon energy of excitation exceeds the band gap, and more laser energy is converted into thermal energy of lattice. The spectra of edge luminescence of the sample C10 are shown in **Figures 15** and **16** with excitation at 222 and 193 nm, respectively. Spectra are marked with numbers, which correspond to the peak intensity of laser radiation in units of MW/cm^2.

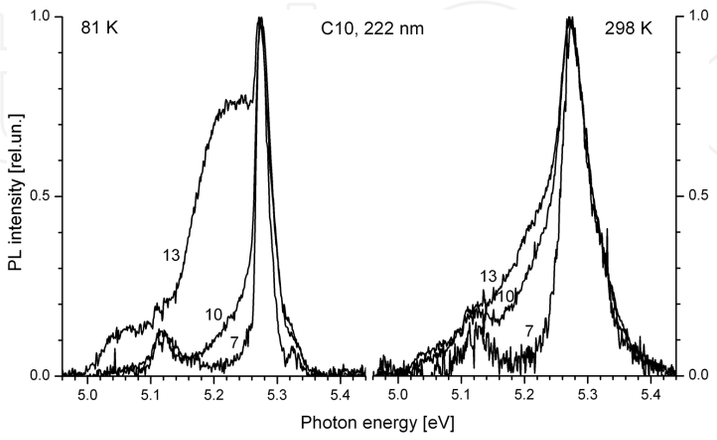

Figure 15. PL spectra of monocrystal CVD diamond sample C10 under the excitation at 222 nm at temperatures of 81 and 298 K. The PL spectra marked by peak intensities [7, 10, and 13 MW/cm^2] of laser radiation on the sample surface.

http://dx.doi.org/10.5772/65064

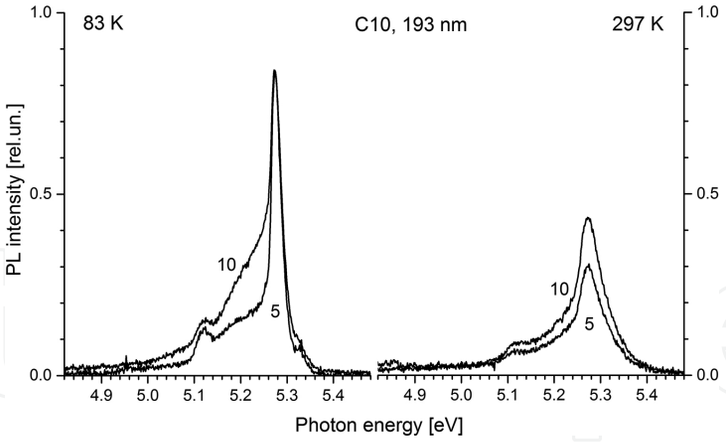

Figure 16. PL spectra of monocrystal CVD diamond sample C10 under the excitation at 193 nm at temperatures of 83 and 297 K. The PL spectra marked by peak intensities [5 and 10 MW/cm^2] of laser radiation on the sample surface.

According to the expression (2) at 222 nm excitation with peak intensities of 7, 10 and 13 MW/cm^2, the peak densities of non-equilibrium carriers were (0.72, 1.04 and 1.35)×10^{18} cm^{-3}, respectively. At 193 nm excitation with peak intensities of 5 and 10 MW/cm^2, the peak densities were (3.47 and 6.94)×10^{18} cm^{-3}, respectively. Thus, for comparable peak densities, the PL spectra, shown in **Figures 15** and **16**, were significantly different.

At 222 nm excitation with the peak intensity 7 MW/cm^2, the FE recombination band was observed only at temperatures of 81 and 298 K in the PL spectrum (see **Figure 15**). At 298 K, there was a considerable thermal broadening of the FE band components. At 10 MW/cm^2 on the long-wavelength edge of the TO-component of FE band, the shoulder appeared due to the EHL radiative recombination (and EC, possibly). When the peak intensity achieved of 13 MW/cm^2 and the sample temperature was 81 K, the EHL band was expressed explicitly as the TO-component at 5.16–5.22 eV and the TO+O$^{\Gamma}$-component at 5.0–5.09 eV. There was possible contribution of TA-component in the spectral range of 5.18–5.26 eV and of EC band in the spectral range of 5.20–5.26 eV. The broadening of short-wavelength edge of TO-component of FE band at 81 K in the spectral range of 5.18–5.34 eV was also due to the contribution of TA-component of EHL band. At the temperature of 298 K, the short-wavelength edge of TO-component of FE band practically did not change with increasing of laser intensity. Note that at the temperatures of liquid nitrogen and of RT, the long-wavelength shoulder of TO-component of FE band was presented in the PL spectrum. At RT, this broadening cannot be described in terms of thermal broadening.

Figure 16 shows the PL spectra excited at 193 nm with a peak intensity of 5 and 10 MW/cm^2 for temperatures 83 and 297 K. At 193 nm PL excitation, the peak density of electron-hole pairs was higher by 3–10 times than at 222 nm excitation. The radiation at 193 nm is absorbed in layer ~13 μm. It was an order of magnitude less than that at 222 nm excitation. However, at 193 nm excitation the PL spectra at 83 K showed a smaller contribution EHL recombination band than at 222 nm excitation. At excitation on the same wavelength, the charge carrier density increase was resulted in the increase in the contribution of the EHL band. Presumably, there is a high density of structural defects in a surface layer, which are nonradiative

recombination centers. It results in an increase in threshold FE density for EHL condensation. At the same time, the envelope of PL spectra essentially unchanged at RT with different peak intensities. Unlike excitation at 222 nm in PL spectra at 193 nm excitation, "tails" in the spectral region of <5.08 eV were observed that for the case of silicon was attributed to the EHP recombination [13].

Figure 17 shows the edge luminescence spectra of the HPHT single crystal C12 at 222 nm excitation. The EHL recombination band was not expressed clearly, and FE band was three times less intensive with the same peak intensities as for sample C10. The spectrum envelopes did not change during the peak intensity growth for both temperatures. This indicates a much greater density of nonradiative recombination centers in the sample C12, as compared to C10, which makes it difficult for EHL condensation in sample C12.

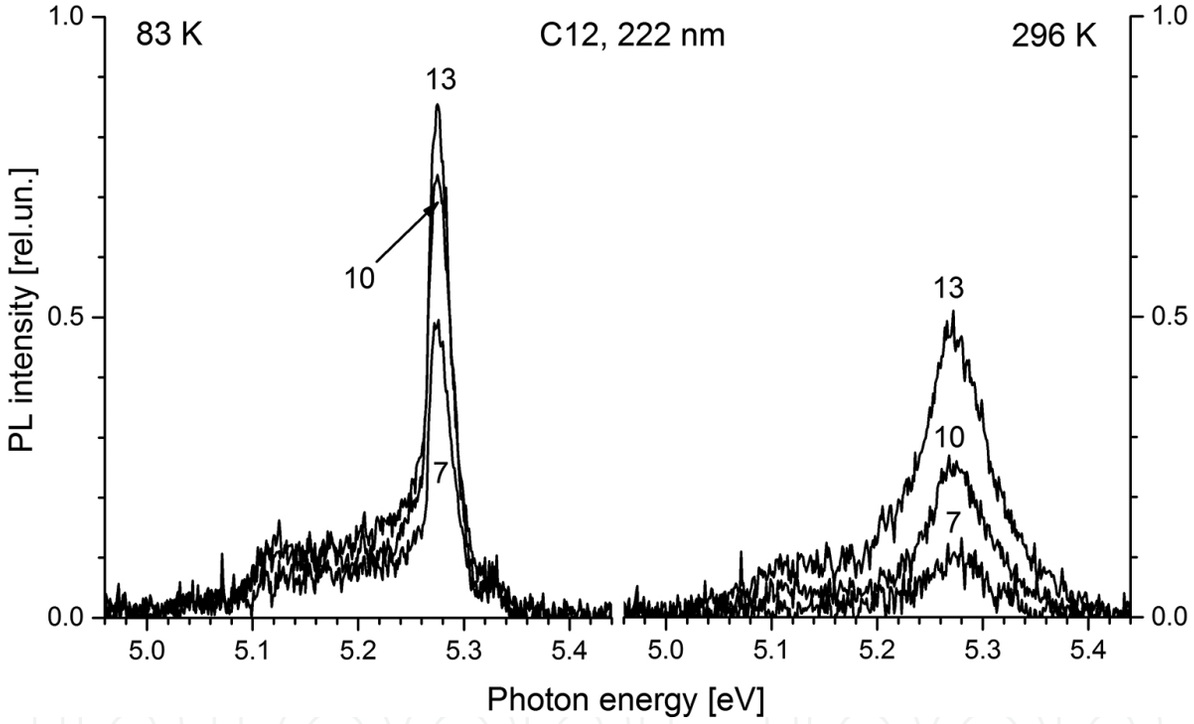

Figure 17. PL spectra of monocrystal HPHT diamond sample C12 under the excitation at 222 nm at temperatures of 83 K and 296 K. The PL spectra peaks are marked by peak intensities [7, 10 and 13 MW/cm^2] of laser radiation on the sample surface.

The EHL condensation was evident also in the temperature dependence of intensity of the dominant TO-component of FE recombination band, as shown in **Figure 18**. In conditions where condensation EHL was insignificant, the maximum of temperature dependence of FE band intensity was close to 150 K (see **Figure 18** for C10, 7 MW/cm^2). The peak position arises from the FE lifetime temperature dependence (Eq. 4). As the EHL band intensity increases with the increase in laser intensity (10 MW/cm^2), the additional maximum appeared at 190–220 K on the temperature dependence. As the intensity increases further (13 MW/cm^2), the maximum at 190–220 K becomes dominant.

http://dx.doi.org/10.5772/65064

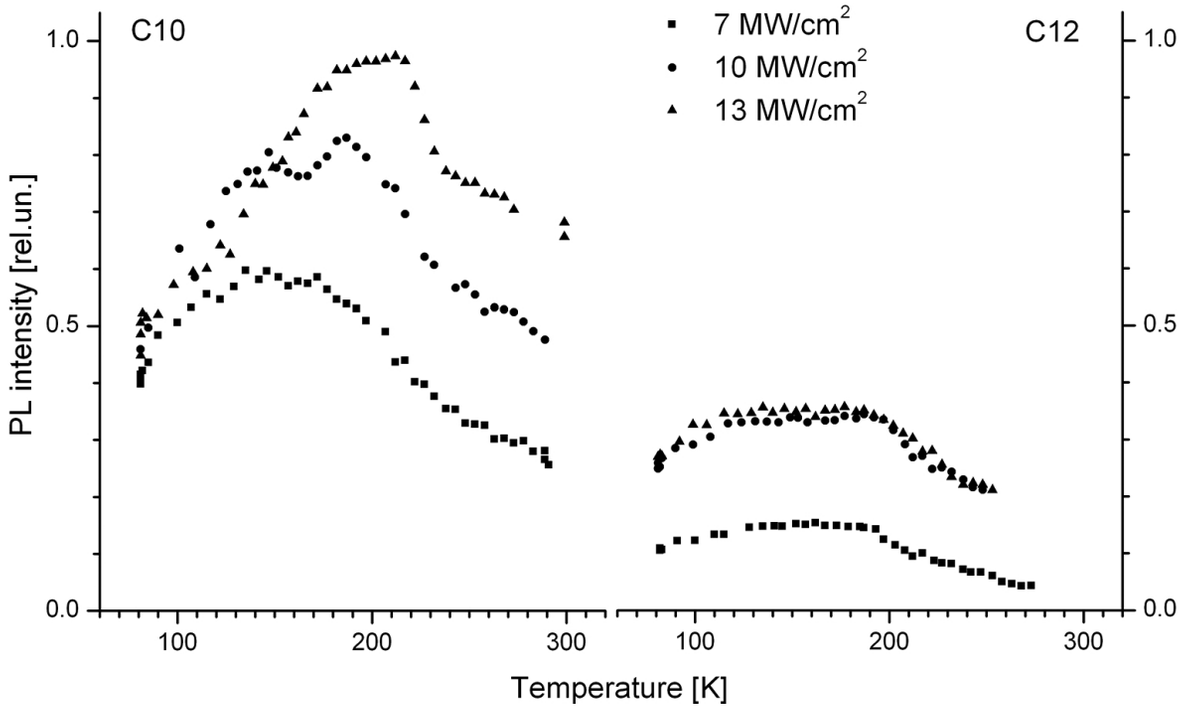

Figure 18. Temperature dependencies of FE recombination band intensities of two monocrystal diamond samples C10 and C12 at different excitation intensities at 222 nm. Squares-laser intensity 7 MW/cm^2, circles-10 MW/cm^2, triangles-13 MW/cm^2.

Note that for the C12 sample (**Figure 18**), the temperature dependences were differed. The FE band intensity remained practically unchanged in the temperature range of 130–190 K, i.e., the temperature maximum has been extended essentially, in contrast to the dependencies for the sample C10. With an increase in the peak laser intensity from 10 to 13 MW/cm^2, the FE recombination intensity remained approximately unchanged. The additional maximum at 190–220 K was not clearly manifested.

The analysis of dependencies in **Figures 17** and **18** leads to the conclusion that:

1. When EHL droplet size increases, the FE density decreases due to their loss in the process of EHL condensation (FE intensity maximum shifts on the temperature dependence);
2. The FE condensation can take place up to temperatures of ~220 K (EHL or EHP according to Mott);
3. The interaction cross-section of nonradiative recombination centers with EHL drops is higher than with FEs (no intensity increase for sample C12 with the peak laser intensity increase from 10 to 13 MW/cm^2).

The plot of phase diagram of electron-hole system in the diamond as the temperature dependence on the charge carrier density is an important problem, which is not completely solved yet. The results of the plot of phase diagram are summarized in **Figure 19**. Experimental data and theoretical models were used in [14, 41, 42].

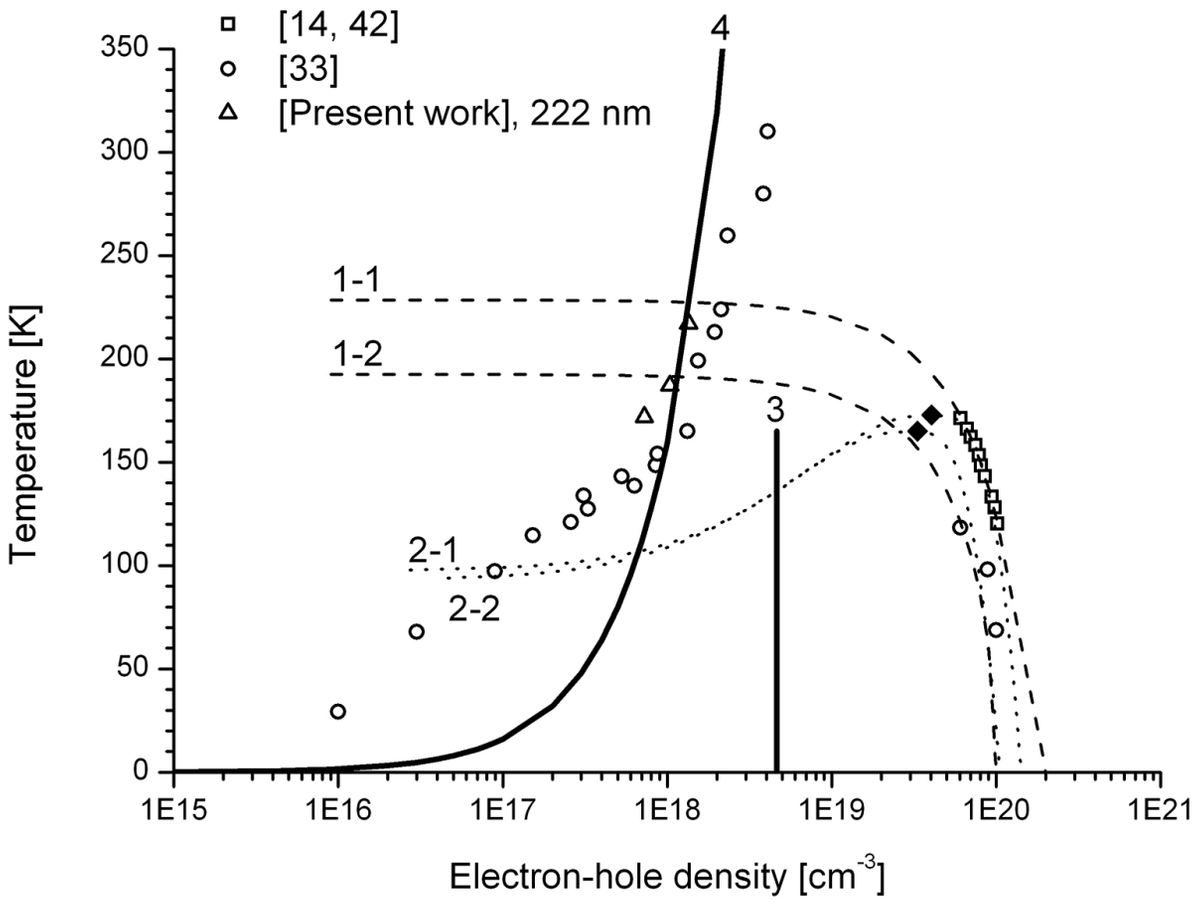

Figure 19. The phase diagram of the electron-hole system in diamond. White squares are experimental data from [14, 42]. White circles are experimental data from Ref. [33]. 1-1-degenerate plasma model T_{crit} = 173 K, n_{crit} = 4.05×10^{19} cm^{-3} from [42], 1-2-degenerate plasma model T_{crit} = 165 K, n_{crit} = 3.33×10^{19} cm^{-3} from [33], 2-1-liquid-gas transition boundary in Guggenheim model T_{crit} = 173 K, n_0 = 1.41×10^{20} cm^{-3} from [42], 2-2—liquid-gas transition boundary in Guggenheim model T_{crit} = 165 K, n_0 = 1.0×10^{20} cm^{-3} from [33], 3-Mott criterion in Thomas-Fermi approximation [33, 42], 4-Mott criterion in Debye-Huckel approximation [33, 42]. Black rhombs are two sets of critical temperature and EHP density: T_{crit} = 160 и 173 K, n_{crit} = (3.33 и 4.05)×10^{19} cm^{-3}. White triangles are experimental data of present work.

The experimental data [14, 42] were approximated (white squares in **Figure 19**) in the model of a degenerate plasma with the critical temperature T_{crit} = 173 K and the critical density n_{crit} = 4.05 10^{19} cm^{-3} (curve 1-1 in **Figure 19**) and in the model of simple liquid near the critical point with the critical temperature T_{crit} = 173 K and the charge carrier density at the absolute zero of temperature n_0 = 1.0×10^{20} cm^{-3} (curve 2-1 in **Figure 19**). Note that in [14, 42] the PL excitation of diamond samples was provided by laser radiation with duration of 5–8 ns at FWHM.

In Refs. [33] and [41], the model of a degenerate plasma was used also with the critical temperature T_{crit} = 160 K and the critical density n_{crit} = 3.33×10^{19} cm^{-3} (curve 1-2 in **Figure 19**) and the model of simple liquid near the critical point [43] with a critical value temperature T_{crit} = 160 K and the charge carrier density at the absolute zero of temperature n_0 = 1.0×10^{20}

cm^{-3} (curve 2-2 in **Figure 19**). In Ref. [33], the laser pulses with subpicosecond duration (200 fs) were used for PL excitation. These experimental data (white circles in **Figure 8**) were obtained not only for right side of the phase diagram at densities higher than the critical, but at densities less than densities of the Mott transition. In Thomas-Fermi approximation, the Mott transition has a threshold (curve 3 in **Figure 19**), but in Debye-Huckel approximation the Mott transition criterion increases monotonically with the FE density (curve 4 in **Figure 19**).

Note that the values of the experimental densities in **Figure 19** were obtained [14, 33, 42] through the form factors analysis of spectral components. But the density range of 4.1×10^{18}–6.0×10^{19} cm^{-3} was not investigated.

Black rhombs in **Figure 19** mark two sets of critical temperature and density for the EHL condensation. Different values of these quantities define the different calculated values in a degenerate plasma model and a phenomenological model of the gas-liquid transition (curves 1-1, 1-2, 2-1, 2-2 in **Figure 19**). As shown in **Figure 20**, the several different values of critical temperature and density for the EHL condensation were defined or calculated for the diamond [16, 31–33] and other semiconductors [30, 32]. Furthermore, in [42] it was postulated that the critical temperature for the EHL condensation is in the range of 180–207 K at PL excitation by laser pulses of nanosecond duration. At the same time, in Ref. [43], the EHL was observed at temperatures below 120 K at PL excitation by subpicosecond laser pulses. Note that the critical EHL condensation temperatures were determined from the shapes of PL spectra, but the EHL critical densities were the calculated parameters. Significant differences between the nanosecond PL excitation [14, 42] and the femtosecond PL excitation [32, 33, 43] were caused by:

1. Different modes of excitation—stationary and pulsed, respectively. At the stationary mode of excitation, the pulse duration is significantly longer than the lifetime of EHL drops (less than 1 ns), which leads to the nucleation of drops during the excitation pulse. At the pulsed mode of excitation, the duration of laser radiation is shorter in three orders of magnitude than the lifetime of EHL drops, so the PL spectra of EHL recombination display drops formed around the same time.

2. Different peak intensities of laser excitation—a few to tens of MW/cm^2 at the stationary mode and a few to tens of GW/cm^2 at the pulsed mode. The peak intensity of laser radiation of gigawatt level leads to the generation of electron-hole plasma with an initial density of more than 10^{20} cm^{-3} and causes the lattice heating due to the thermalization process of hot carriers and to the Auger recombination. This heating leads to a decrease in the critical temperature for the EHL condensation. For example, the authors of [44] were forced to use the understated initial FE density of 10^{18} cm^{-3} to perform calculations.

3. Different excitation wavelengths—218–220 and 215 nm, respectively. Due to the sharp increase in the absorption coefficient at the fundamental absorption edge of diamond [3], the shorter wavelengths are characterized by the thinner diamond layer in which absorption occurs. Therefore, at the same radiation intensity the shortwave radiation creates the higher initial FE density (see **Figure 2**). Moreover, the FE generation by shortwave photons

creates "hot" carriers, which transmit more energy to the diamond lattice in the thermalization process, and it reduces the critical temperature.

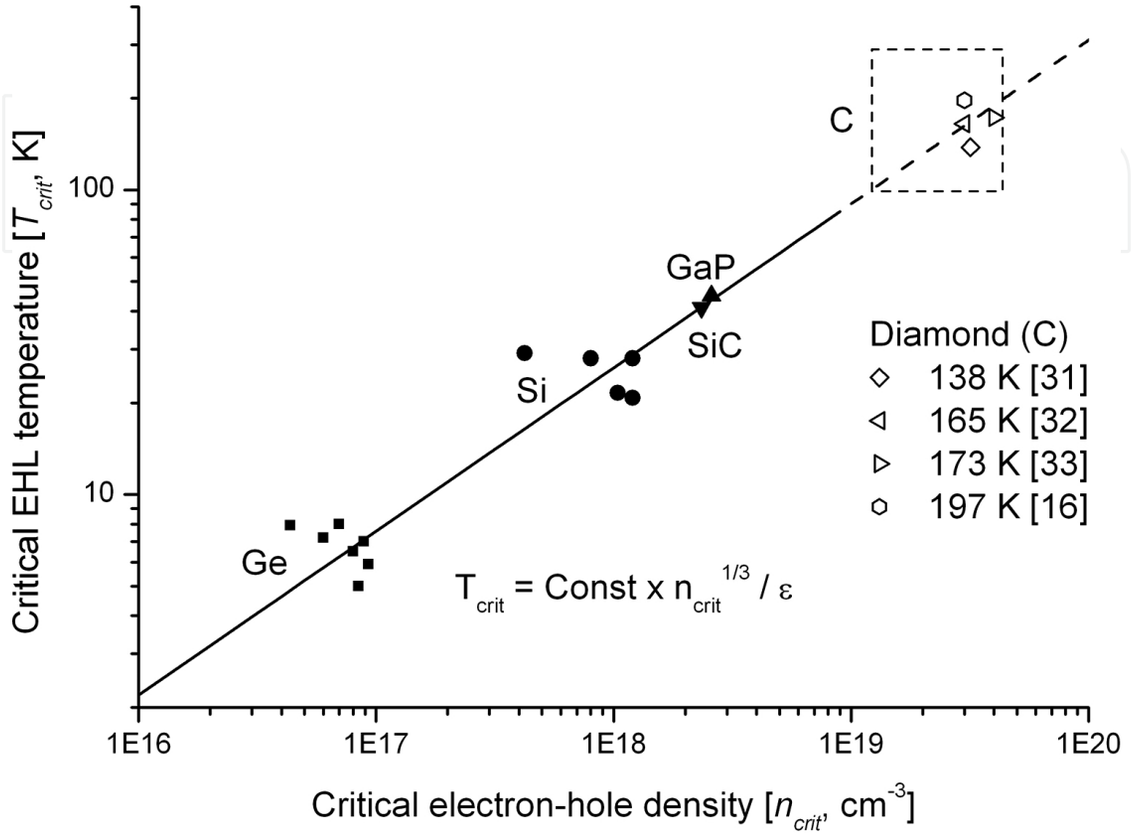

Figure 20. Critical EHL temperatures versus critical EHL densities in the several semiconductors. Black squares-germanium (Ge), black circles-silicon (Si), black down triangle-silicon carbide (SiC), black up triangle-gallium phosphite (GaP), white shapes-diamond (C). Data for Ge, Si, SiC and GaP referred to [30, 32], data for C (diamond)—[16, 31–33].

As it can be seen from **Figure 19**, the modeling of phase diagram of gas FE-EHL in the diamond describes satisfactorily the right branch, whereas, for the left branch the used models do not give a close description of experimental curves. The Mott criterion in Debye-Huckel approximation describes most closely the boundary of FE gas existence (left branch of the phase diagram) at the FE densities of (1–4)×10^{18} cm^{-3}. The values of critical temperatures and densities of experimental data of this work are marked as white triangles in **Figure 19**. Note that we have obtained the charge carrier densities according to expressions (1) and (2), but the values of critical temperature were taken from the positions of maxima on the temperature dependences of FE intensity (**Figure 18**).

Thus, the study of the EHL properties in the diamond has not yet responded to the key issues related to the conditions of condensation, evaporation and recombination. It remains still unclear what values of critical temperature and charge carrier density take place, and what their dependences on the impurity-defective composition of samples, the excitation energy of particles and the duration of excitation pulses are like. The phase diagram of EHL existence requires the additional data in the density range of 4.0×10^{18}–6.0×10^{19} cm^{-3}. An important aspect

is to determine the temperature dependence of intensities of TA- and TO+O^{Γ}-components of EHL recombination band. Does EC band give a contribution to PL spectra (their position, intensity)? In addition, there are two different concentrated states of nonequilibrium charge carriers in the diamond—EHL and EHP—which can have the same densities under certain conditions. So, the question arises: what are the differences between these two states?

6. Applications of recombination radiation in the diamond

The most obvious application of recombination radiation in the diamond is producing of light emitting devices (LED) based on diamond. The recombination radiation in the luminescence spectrum of diamond is located in the spectral range of 230–245 nm near the fundamental absorption edge (225 nm) (see Section 3). The band-A of luminescence is located in the blue region of the visible spectrum with the maximum at 440 nm and has the recombination origin (see Section 4).

The LED's operating principle is based on the phenomenon of electroluminescence (EL)-radiative recombination of electron-hole pairs injected through contacts. The problem of making ohmic contacts to the diamond is solved in general [44]. Typically, the ohmic contacts to the diamond consist of three-layer metal deposition: carbide-former metal (Ti, Ta, Mo, W, Cr), interdiffusion-blocking layer (Pt) and protective/mounting layer (Au).

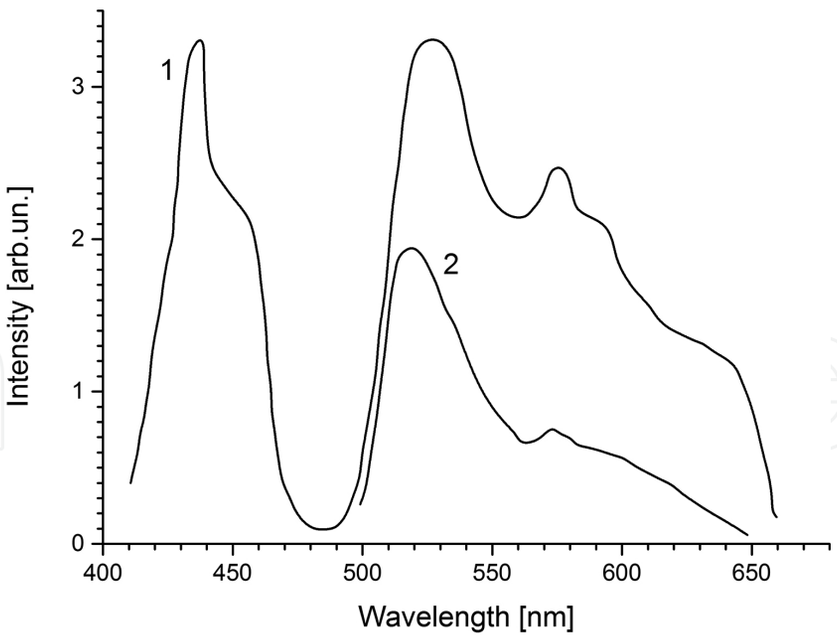

Figure 21. EL spectra of two natural diamond samples of IIb type referred to [46]. 1-sample without PL, 2-sample with yellow-green PL.

The first reports on EL in diamond were about semiconductor IIb type samples which were naturally doped with boron. The impurity of boron is an acceptor in diamond with an

activation energy of 0.38 eV. In Ref. [45], the observation of the blue EL band of natural diamond sample with the maximum at 440 nm (the spectrum is not given) was reported. The EL was observed only at one polarity of bias of 50–100 B. In Ref. [46], a broadband EL (see **Figure 21**) was observed for several natural diamonds, presumably of IIb type (only a small fraction of the samples gave EL). In addition to the blue band with the maximum at 440 nm, the EL spectra of samples showed a broadband with several local maxima in the range from 500 to 650 nm. The green band of EL is appeared in the EL spectrum with a significant delay (tens of minutes). In general, the EL has demonstrated strong intensity fluctuations and has quenched when sample was cooled to a temperature below 100 K. This fact involves hopping conduction. In Ref. [47], the production of LED based on natural and HPHT diamonds was reported. The p- and n-types of conductivity were created by ion implantation of boron and lithium, respectively. The emission spectrum of resulting p-n transition is shown in **Figure 22**. The intensity of this transition decreases to zero with increasing temperature from -200 to 300°C, i.e., the band-A of luminescence took place.

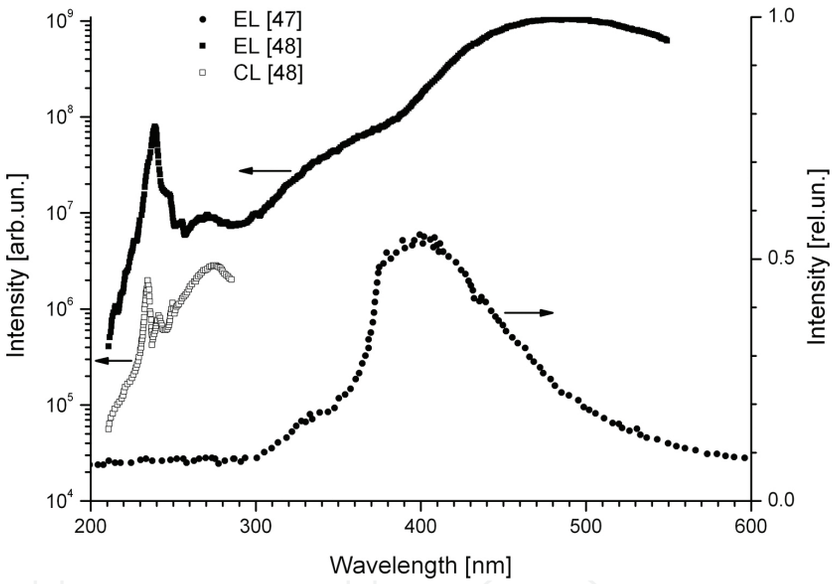

Figure 22. EL and CL luminescence spectra of diamond-based junctions referred to [47, 48]. The EL spectrum of p-n junction from [47] is showed by black circles. The p- and n-types of conductivity were created in the natural diamond by ion implantation of boron and lithium, respectively. The EL spectrum of diamond LED from [48] showed by black squares. The p- and n-types of conductivity were created in the CVD diamond during the synthesis process using admixtures of boron and phosphorus, respectively. The CL spectrum of the LED is shown as white squares.

The development of CVD-diamond synthesis and the ability to create p- (boron) and n- (0.47 eV phosphorus, lithium 0.29 eV) types of sample conductivity during the synthesis or during the subsequent ion implantation have led to reports on the EL research of CVD diamonds and the creation of LED based on various types of light-emitting junctions in diamond [48–62]. The voltage of only tens of volts was used.

In 2002, the first reports on diamond LED development, emitting in the UVC range at 235 nm, appeared. In Ref. [48], a diamond LED p-n junction was reported. The spectrum of LED emitted

radiation is shown in **Figure 22**. The FE emission at 235 nm was characterized by intensity of an order of magnitude less than the intensity of band-A. So, the low intensity of FE band indicates the unsatisfactory quality of doped layers. In Ref. [49], a similar device showed the same characteristics: the presence of FE peak at 235 nm and the intense band-A.

In Refs. [50] and [51], the three-layer structure diamond:N-diamond:Ce-SiO_2 was studied. The EL spectrum showed the presence of wide and narrow bands in the spectral region 300–630 nm, arising from the band-A, transitions in cesium atoms and nitrogen complexes. The monotonically decreasing tail was observed from 630 nm to the IR region. This structure demonstrated the brightness of 3.5 cd/m^2 at RT and voltage of 150 V. In Ref. [52], the p-n junction was formed in a CVD single crystal by ion implantation of boron and lithium with subsequent ion implantation of xenon. The resulting device demonstrated the EL broadband in the spectral region from 450 to 850 nm at voltage 100 V and RT. There were the vibronic system of Xe centers with ZPL at 812.5 nm and the weak emission of N-V centers with ZPL at 575 nm.

In Ref. [53], a diamond-based p-i-p structure was described, which showed the EL emission at 235 nm. Later the same group produced a p-i-p-i-p device emitting FE recombination band [54]. In Ref. [55], a p-i-n transition doped with boron and phosphorus diamond layers was reported. At voltages of ±15 V, the p-i-n transition showed the dominant FE band at 235 nm, but the band-A was suppressed. In Ref. [56], the C-Si heterojunction demonstrated the red EL at RT. In Ref. [57], by ion implantation of B, As and P the p+-p-n structure was fabricated, which was based on p-type HPHT diamond. At RT the p+-p-n structure demonstrated the effect of superluminescence in the spectral region of band-A. In Ref. [58], the p-C/n-AlN-heterojunction showed the dominant FE recombination band at 235 nm in the diamond layer. In [59] the p-i-n structure based on boron and phosphorus (ion implanted) CVD diamond layers showed the EL of N-V defects at 575 nm. The authors of [60] suggested the method of creating graphite electrodes buried in a CVD diamond volume by the action of a focused MeV-ion beam (He^+). In the EL spectrum, there were the band-A, the ZPL at 575 nm of N-V centers, ZPL at 536.3 and 560.5 nm centers associated with helium and the broadband at 740 nm of Si-V or V centers.

We note that due to the superior thermal conductivity (higher than of copper in 5 times), the diamond samples are used also as passive heat sinks for LEDs based on other semiconductor materials [61, 62].

At the time being diamond LEDs are not widely used. The main reason is the need to improve the quality of the diamond structures. Another reason-the fundamental: diamond is a semiconductor with indirect-band structure, which reduces the efficiency of FE radiative recombination. At the same time, theoretical searches of ways to overcome the fundamental limitations of the diamond as a material for LEDs are being conducted. In [63] it was proposed to change the band structure of diamond to the direct-gap by using the linear compression of ~4% or lattice deformation by high doses of radiation damage. In [64] it was suggested to generate picosecond high-power pulses at 235 nm by using the superluminescence in diamond-cooperative spontaneous FE radiative recombination. The superluminescence is possible to be created in a ring resonator. At this condition, the Mott transition is not achieved.

Thus, the recombination radiation of diamond in the FE band (235 nm) or the band-A (400–650 nm) may be applied in LEDs. Despite the fact that the EHL is an interesting phenomenon in terms of quantum effects, its practical use as a radiation source or any other thing has not been found. The situation is the same for all semiconductors. At the same time, diamond has a highest critical temperature of EHL condensation (>160 K), which still gives hope for the practical application.

In Ref. [38], the strengthening of photoconductivity in the CVD diamond under conditions of EHL existing was reported. Unlike a single FE, drops of EHL are not electrically neutral particle clusters. Due to the different work function of electrons and holes (due to the different effective masses), the EHL drops have a noncompensated surface charge [13]. Consequently, the EHL drops may drift in the electric field and participate in the photocurrent. One can assume that the EHL drops in diamond could be used as controlled sources of photons, dynamic quantum dots, etc.

7. Conclusion

This chapter provides the original experimental data on the recombination radiation of natural and synthetic diamonds and the overview of the literature about.

The FE recombination radiation in the diamond is observed in CL, PL and EL spectra in the shape of the four-component band containing TA-, TO-, LO- and TO+O^{Γ}-components at 5.325, 5.275, 5.254 and 5.117 eV, respectively. The "non-diamond" carbon phase and impurity-defect centers have the negative effect on the intensity of FE recombination band. The spectral position of FE band maximum at 5.275 eV did not change within the measurement error in the temperature range of 80–300 K, which contradicts the phenomenon of band gap decreasing with the increase in temperature. At low excitation levels, the temperature dependence of the FE recombination band intensity has the maximum at ~150 K, which is in agreement with published data. The band-A, caused by intrinsic defects of the structure containing the sp^2-hybridized carbon bonds, is located in the spectral range of 350–650 nm with the maximum at about 440 nm and is characterized by the decay time of 8–19 ms in the temperature range of 80–300 K. The band-A reflects the perfection degree of diamond sample, i.e., the higher the band-A intensity is, the greater the structure defect density is. There is a competition between the band-A and FE recombination band in diamond. The emission spectrum of the band-A may be imposed by vibronic bands of N_3V, N_2V, NV centers, which are characterized by decay times in the nanosecond time range. Therefore, the measurement of luminescence emission spectra with time resolution allows to separate in time the spectra of band-A and other structural defects.

The recombination radiation of EHL drops in diamond is observed in CL and PL spectra at temperatures ≤200 K and peak carrier densities ≥$(0.3–1.0)\times10^{18}$ cm^{-3}. The EHL band consists of three phonon components: TA, TO and TO+O^{Γ} at 5.249, 5.211 and 5.075 eV, respectively. The dominant TO-component of EHL band begins to appear in the form of long-wavelength shoulder of TO-component of FE band when the charge carrier density reaches the critical

value. A further increase in carrier density leads to an increase in EHL band intensity. The surface layer of diamond sample is more defective than the inner volume. Therefore, the absorption of exciting radiation in a thin layer hampers EHL condensation compared with volume absorption. The EHL condensation results in displacement of FE band intensity maximum on the temperature dependence to higher temperatures up to 220 K, which can be interpreted as a decline of excitons in the EHL condensation process at lower temperatures. In this context, the critical temperature of EHL condensation is not established and, presumably, takes values in the range of 160–220 K. In this regard, the phase diagram of EHL existence requires clarification.

Currently, fabricated LEDs based on p-n, p-i-n, p-i-p and other junctions in diamond structures have showed the possibility of spontaneous emission in the UV range at 235 nm and in the visible range of 400–800 nm. However, the diamond LEDs do not satisfy the requirements of efficiency and emission brightness. The main reason is the indirect-band zone structure of diamond, which leads to a long FE lifetime and low efficiency of the three-particle radiative recombination. To overcome this fundamental limitation, it was suggested to use the local deformation of the crystal, resulting in direct-gap zone structure in diamond and the super-luminescence in the ring resonator. The prospect of finding the solution to increase the efficiency and the emission brightness of the diamond-based LEDs is associated with the possibility of obtaining the compact devices that are emitting in the UV-C spectrum.

Acknowledgements

This report was prepared with the support of the Russian Foundation for Basic Research, Project No. 14-02-31132.

Author details

Evgeniy Igorevich Lipatov*, Dmitriy Evgen'evich Genin, Denis Valer'evich Grigor'ev and Victor Fedotovich Tarasenko

*Address all correspondence to: lipatov@loi.hcei.tsc.ru

Institute of High Current Electronics SB RAS, Tomsk, Russian Federation

References

[1] Pelant I, Valenta J. Luminescence spectroscopy of semiconductors. New York: Oxford University Press; 2012. 542 p. doi:10.1093/acprof:oso/9780199588336.001.0001

[2] Ruf T, Cardona M, Sternschulte H, et al. Cathodoluminescence investigation of isotope effects in diamond. Solid State Communications. 1998;105:311–316. doi:10.1016/S0038-1098(97)10196-X

[3] Lipatov EI, Genin DE, Tarasenko VF. Optical spectra and electron–hole liquid in diamond. Optics and Spectroscopy. 2015;119:918–923, doi:10.1134/S0030400X15120164

[4] Lipatov EI, Avdeev SM, Tarasenko VF. Photoluminescence and optical transmission of diamond and its imitators. Journal of Luminescence. 2010;130:2106. doi:10.1016/j.jlumin.2010.06.001

[5] Novikov N.V, editor. Handbook of Physical Properties of Diamond (in Russian). Kiev: Naukova dumka; 1987. 1132 p.

[6] Salvatori S., Pace E., Rossi MC, Galluzzi F. Photoelectrical characteristics of diamond UV detectors: dependence on device design and film quality. Diamond and Related Materials. 1997;6:361. doi:10.1016/S0925-9635(96)00757-1

[7] Lipatov EI, Lisitsyn VM, Oleshko VI, et al. Pulsed cathodoluminescence of natural and synthetic diamonds excited by nanosecond and subnanosecond electron beams. In: Yamamoto N, editor. Cathodoluminescence. Rijeka, Croatia: InTech; 2012. p. 51–70. doi: 10.5772/1989

[8] Yokota Y, Tachibana T, Miyata K, et al. Cathodoluminescence of boron-doped hetero-epitaxial diamond films on platinum. Diamond and Related Materials. 1999;8:1587–1591. doi:10.1016/S0925-9635(99)00085-0

[9] Sharp SJ, Collins AT, Davies G, Joyce GS. Higher resolution studies of shallow bound exciton luminescence in diamond. Journal of Physics: Condensed Matter. 1997;9:L451–L455. doi:10.1088/0953-8984/9/33/003

[10] Gaman VI. Physics of semiconductor devices: Tutorial (in Russian). Tomsk: NTL Publishing House; 2000. 426 p.

[11] Clark CD, Dean PJ, Harris PV. Intrinsic edge absorption in diamond. Proceedings of the Royal Society of London A. 1964;277:312–329. doi:10.1098/rspa.1964.0025

[12] Robins LH, Farabaugh EN, Feldman A. Cathodoluminescence spectroscopy of free and bound excitons in chemical-vapor-deposited diamond. Physical Review B. 1993;48:14167–14181. doi:10.1103/PhysRevB.48.14167

[13] Keldysh LV. The electron-hole liquid in semiconductors. Contemporary Physics. 1986;27:395–428. doi:10.1080/00107518608211022

[14] Sauer R, Teofilov N, Thonke K. Exciton condensation in diamond. Diamond and Related Materials. 2004;13:691–699. doi:10.1016/j.diamond.2003.10.005

[15] Teofilov N, Sauer R, Thonke K, Koizumi S. Bound exciton luminescence related to phosphorus donors in CVD diamond. Physica B. 2003;340–342:99–105. doi:10.1016/j.physb.2003.09.011

[16] Lipatov EI, Genin DE, Tarasenko VF. Recombination radiation in synthetic and natural diamonds exposed to pulsed UV laser radiation. Russian Physics Journal. 2015;58:911–922. doi:10.1007/s11182-015-0590-x

[17] Takiyama K, Abd-Elrahman MI, Fujita T, Oda T. Photoluminescence and decay kinetics of indirect free excitons in diamonds under the near-resonant laser excitation. Solid State Communications. 1996;99:793–797. doi:10.1016/0038-1098(96)00309-2

[18] Fujii A, Takiyama K, Maki R, Fujita T. Lifetime and quantum efficiency of luminescence due to indirect excitons in a diamond. Journal of Luminescence. 2001;94–95:355–357. doi:10.1016/S0022-2313(01)00299-X

[19] Sobolev EV, Dubov YuI. On origin of diamond roentgenoluminescence (in Russian). Soviet Physics-Solid State. 1975;17:1142.

[20] Dean PJ. Bound excitons and donor-acceptor pairs in natural and synthetic diamond. Physical Review. 1965;139:588–602. doi:10.1103/PhysRev.139.A588

[21] Manfredotti C, Fizzotti F, Lo Giudice A, et al. Ion beam induced luminescence maps in CVD diamond as obtained by coincidence measurements. Diamond and Related Materials. 1999;8:1592–1596. doi:10.1016/S0925-9635(99)00051-5

[22] Walker J. Optical absorption and luminescence in diamond. Reports on Progress in Physics. 1979;42:1607–1659. doi:10.1088/0034-4885/42/10/001

[23] Prins JF. Recombination luminescence from defects in boron-ion implantation-doped diamond using low fluencies. Materials Research Innovations. 1998;1:243–253.

[24] Lawson SC, Kanda H, Kiyota H, et al. Cathodoluminescence from high-pressure synthetic and chemical-vapor-deposited diamond. Journal of Applied Physics. 1995;77:1729–1734. doi:10.1063/1.358865

[25] Nadolinny VA, Yureva OP, Eliseev AP, et al. The destruction of the nitrogen B1-centers in plastic deformation of natural diamonds of IaB type and the behavior of formed defects in the P,T-processing (in Russian). Doklady Akademii Nauk. 2004;399:532–536.

[26] Anoikin E, Muhr A, Bennett A, et al. Diamond optical components for high-power and high-energy laser applications. In: Proceedings of the SPIE; 2015. p. 93460T-1

[27] Takeuchi D, Watanabe H, Yamanaka S, et al. Origin of band-A emission in diamond thin films. Physical Review B. 2001;63:245328. doi:10.1103/PhysRevB.63.245328

[28] Cleri F, Keblinski P, Colombo L, et al. On the electrical activity of sp^2-bonded grain boundaries in nanocrystalline diamond. Europhysics Letters. 1999;46:671–677. doi:10.1209/epl/i1999-00318-5

[29] Lipatov EI, Tarasenko VF, Lisitsyn VM, Oleshko VI. Spectral and kinetic characteristics of the pulsed cathodoluminescence of a natural IIA-type diamond. Russian Physics Journal. 2007;50:52–57. doi:10.1007/s11182-007-0005-8

[30] Tikhodeev SG. The electron-hole liquid in a semiconductor, Soviet Physics Uspekhi. 1985;28:1–30.

[31] Vouk MA. Conditions necessary for the formation of the electron-hole liquid in diamond and calculation of its parameters. Journal of Physics C: Solid State Physics. 1979;12:2305–2312. doi:10.1088/0022-3719/12/12/016

[32] Shimano R, Nagai M, Horiuch K, Kuwata-Gonokami M. Formation of a high Tc electron-hole liquid in diamond. Physical Review Letters. 2002;88:057404. doi:10.1103/PhysRevLett.88.057404

[33] Nagai M, Shimano R, Horiuchi K, Kuwata-Gonokami M. Phase diagram of the quantum degenerate electron–hole system in diamond. Physica Status Solidi (b). 2003;238:509–512. doi:10.1002/pssb.200303171

[34] Thonke K, Schliesing R, Teofilov N, et al. Electron-hole drops in synthetic diamond. Diamond and Related Materials. 2000;9:428–431.doi:10.1016/S0925-9635(99)00315-5

[35] Kozak M, Trojanek F, Popelar T, Maly P. Dynamics of electron-hole liquid condensation in CVD diamond studied by femtosecond pump and probe spectroscopy. Diamond and Related Materials. 2013;34:13–18. doi:10.1016/j.diamond.2013.01.008

[36] Nakazawa K, Umezawa H, Tachiki M, Kawarada H. Non-linear increases in excitonic emission in synthetic type-IIa diamond. Diamond and Related Materials. 2003;12:1995–1998. doi:10.1016/S0925-9635(03)00194-8

[37] Saarela M, Taipaleenmaki T, Kusmartsev FV. Clustering of the electron-hole liquid. Physica E: Low-Dimensional Systems and Nanostructures. 2003;18:339–340. doi:10.1016/S1386-9477(02)01078-0

[38] Lipatov EI, Genin DE, Tarasenko VF. Pulse photoconductivity of diamond at the quasi-stationary laser excitation at 222 nm under the conditions of existence of the electron-hole liquid. JETP Letters. 2016;103:663–668.

[39] Kozak M, Trojanek F, Maly P. Large prolongation of free-exciton photoluminescence decay in diamond by two-photon excitation. Optics Letters. 2012;37:2049–2051. doi:10.1364/OL.37.002049

[40] Ivakin EV, Kisialiou IG, Ralchenko VG, et al. Investigation of free charge carrier dynamics in single-crystalline CVD diamond by two-photon absorption. Quantum Electronics. 2014;44:1055–1060. doi:10.1070/QE2014v044n11ABEH015540

[41] Nagai M, Shimano R, Horiuchi K, Kuwata-Gonokami M. Creation of supercooled exciton gas and transformation to electron-hole droplets in diamond. Physical Review B: Condensed Matter and Materials Physics. 2003;68:081202. doi:10.1103/PhysRevB.68.081202

[42] Teofilov N, Schliesing R, Thonke K, et al. Optical high excitation of diamond: phase diagram of excitons, electron-hole liquid and electron-hole plasma.

Diamond and Related Materials. 2003;12:636–641. doi:10.1016/S0925-9635(02)00386-2

[43] Naka N, Omachi J, Sumiya H, et al. Density-dependent exciton kinetics in synthetic diamond crystals. Physical Review B: Condensed Matter and Materials Physics. 2009;80:035201. doi:10.1103/PhysRevB.80.035201

[44] Werner M. Diamond metallization for device applications. Semiconductor Science and Technology. 2003;18:S41–S46. doi:10.1088/0268-1242/18/3/306

[45] Wolfe R, Woods J. Electroluminescence of semiconducting diamonds. Physical Review. 1957;105:921–922.

[46] Korsun' VM, Mal'tsev EK, Perekrestova LG, et al. Certain characteristics of electroluminescence in natural diamonds. Journal of Applied Spectroscopy. 1969;11:1211–1213.

[47] Melnikov AA, Denisenko AV, Zaitsev AM. Electrical and optical properties of light-emitting p-i-n diodes on diamond. Journal of Applied Physics. 1998;84:6127–6134. doi: 10.1063/1.368880

[48] Koizumi S., Watanabe K., Hasegawa M., Kanda H. Formation of diamond p-n junction and its optical emission characteristics. Diamond and Related Materials. 2002;11:307–311. doi:10.1016/S0925-9635(01)00537-4

[49] Wang WL, Liao KJ, Cai CZ, et al. Ultraviolet electroluminescence at room temperature from a pn junction of heteroepitaxial diamond film by CVD // Diamond and related materials. 2003;12:1385–1388. doi:10.1016/S0925-9635(03)00111-0

[50] Wang X, Wang L, Zhang Q, et al. Electroluminescence spectrum shift with switching behaviour of diamond thin films. Chinese Physics Letters. 2003;20:1868–1870.

[51] Wang X, Wang L, Zhang B, et al. Electroluminescence of diamond:Ce thin films. Semiconductor Science and Technology. 2003;18:144–146.

[52] Zaitsev AM, Bergman AA, Gorokhovsky AA, Huang M. Diamond light emitting diode activated with Xe optical centers. Physica Status Solidi. A: Applications and Materials Science. 2006;203:638–642. doi:10.1002/pssa.200521125

[53] Yamamoto M, Watanabe T, Hamada M, et al. Electrical properties of high-quality CVD diamond p-i-p structures at high electric fields. Applied Surface Science. 2005;244:310–313. doi:10.1016/j.apsusc.2004.10.136

[54] Watanabe T, Teraji T, Ito T. Fabrication of diamond p-i-p-i-p structures and their electrical and electroluminescence properties under high electric fields. Diamond and Related Materials. 2007;16:112–117. doi:10.1016/j.diamond.2006.04.003

[55] Makino T, Tokuda N, Kato H, et al. Electrical and light-emitting properties of (001)-oriented homoepitaxial diamond p-i-n junction. Diamond and Related Materials. 2007;16:1025–1028. doi:10.1016/j.diamond.2007.01.024

[56] Yang D, Chen J, Sekiguchi T, et al. Enhanced red electroluminescence from a polycrystalline diamond film/Si heterojunction structure. Applied Physics Letters. 2007;90:161123. doi:10.1063/1.2730584

[57] Buga SG, Blank VD, Bormashov VS, et al. P-n junction on high-pressure-high-temperature grown single crystal diamond: UV-emission spectra and electrical properties. Journal of Physics: Conference Series. 2008;121/3:032005. doi:10.1088/1742-6596/121/3/032005

[58] Kazuyuki H, Yoshitaka T, Makoto K. Electroluminescence and capacitance-voltage characteristics of single-crystal n-type AlN (0001)/p-type diamond (111) heterojunction diodes. Applied Physics Letters. 2011;98:011908–3. doi:10.1063/1.3533380

[59] Lohrmann A, Pezzagna S, Dobrinets I, et al. Diamond based light-emitting diode for visible single-photon emission at room temperature. Applied Physics Letters. 2011;99:251106. doi:10.1063/1.3670332

[60] Forneris J, Battiato A, Gatto Monticone D, et al. Electroluminescence from a diamond device with ion-beam-micromachined buried graphitic electrodes. Nuclear Instruments and Methods in Physics Research Section B. 2015;348:187–190. doi:10.1016/j.nimb.2014.12.036

[61] Man W, Sun L, Xie P, et al. Microwave CVD diamond thin film for led heat spreader. Diamond and Abrasives Engineering. 2008;2:1–4.

[62] Vilisov AA, Remnev GE, Linnik SA. Light-emitting diode with CVD diamond heat sink (in Russian). Russian Physics Journal. 2013;56:169–171.

[63] Hora H, Prelas MA. Theoretical aspects of diamond films and laser action. Diamond and Related Materials. 1995;4:1376–1382. doi:10.1016/0925-9635(95)00325-8

[64] Kukushkin VA. Simulation of ultraviolet- and Soft X-ray-pulse generation as a result of cooperative recombination of excitons in diamond nanocrystals embedded in a polymer film. Semiconductors. 2013;47:1442–1446. doi:10.1134/S1063782613110122